ELSEVIER

Contents lists available at ScienceDirect

Theoretical and Applied Mechanics Letters

journal homepage: www.elsevier.com/locate/taml



A two-scale method to include essential behaviour of bolted connections in structures including elevated temperatures



Qingfeng Xu^a, Hèrm Hofmeyer^{a,*}, Johan Maljaars^{a,b}

- ^a Eindhoven University of Technology, Eindhoven, 5612 AE, The Netherlands
- ^b TNO, Delft, 2628 CK, The Netherlands

ARTICLE INFO

Keywords: Two-scale method Finite element model Bolted connection Structural failure Elevated temperatures Fire

ABSTRACT

A two-scale method is proposed to simulate the essential behavior of bolted connections in structures including elevated temperatures. It is presented, verified, and validated for the structural behavior of two plates, connected by a bolt, under a variety of loads and elevated temperatures. The method consists of a global-scale model that simulates the structure (here the two plates) by volume finite elements, and in which the bolt is modelled by a spring. The spring properties are provided by a small-scale model, in which the bolt is modelled by volume elements, and for which the boundary conditions are retrieved from the global-scale model. To ensure the smallscale model to be as computationally efficient as possible, simplifications are discussed regarding the material model and the modelling of the threads. For the latter, this leads to the experimentally validated application of a non-threaded shank with its stress area. It is shown that a non-linear elastic spring is needed for the bolt in the global-scale model, so the post-peak behavior of the structure can be described efficiently. All types of bolted connection failure as given by design standards are simulated by the two-scale method, which is successfully validated (except for net section failure) by experiments, and verified by a detailed system model, which models the structure in full detail. The sensitivity to the size of the part of the plate used in the small-scale model is also studied. Finally, multi-directional load cases, also for elevated temperatures, are studied with the twoscale method and verified with the detailed system model. As a result, a computationally efficient finite element modelling approach is provided for all possible combined load actions (except for nut thread failure and net section failure) and temperatures. The two-scale method is shown to be insightful, for it contains a functional separation of scales, revealing their relationships, and consequently, local small-scale non-convergence can be handled. Not presented in this paper, but the two-scale method can be used in e.g. computationally expensive twoway coupled fire-structure simulations, where it is beneficial for distributed computing and densely packed bolt configurations with stiff plates, for which a single small-scale model may be representative for several connections.

1. Introduction. For building structures under fire, strength, stiffness, and stability need to be quantified. This is often carried out by small-scale standard fire tests combined with theoretical models. However, as will be explained below, several issues exist for this approach, and full-scale experiments may be used instead. For example, Lou et al. [1] investigated the progressive collapse of a full-scale steel portal frame exposed to natural fires. To show the importance of carrying out full-scale experiments, with realistic fires, it was also found that the temperature distribution along the height was significantly different from the case loaded by a standard ISO fire. Similarly, Rackauskaite et al. [2] compared the behavior of full-scale multi-storey steel frames subject to either uniform or travelling (i.e. the fire front spreads across the storey or even the complete building) fires. Their results confirmed that to obtain accurate strength, stiffness, and stability predictions, standard fire tests have their limitations and full-scale building experiments are needed.

Unfortunately, a full-scale experiment is expensive, more so for large structures, and a variation of even small factors, like the type of the connections, the presence of glue [3], or pyrolysis [4] may greatly affect the outcomes, rendering the experiments too specific for generic use [5]. For instance, Kodur et al. [6], Cbov et al. [7], and Fisher et al. [8] showed that connections significantly influence the response of structures during a fire. Furthermore, in a research of several cases in which buildings experienced a fire-induced collapse, Beitel et al. [9] concluded that both structural interaction—the mutual effect of components on each other—and the response of the connections played major roles in the failure behavior. De Boer et al. [10] concluded that the failure of bolts and screws can have a detrimental influence on the structural integrity, even causing the fire scenario to change. As such, some researchers developed new approaches to increase the ductility and loading resistance of conventional connections [11,12]. Last but not least, empirical studies

^{*} Corresponding author.

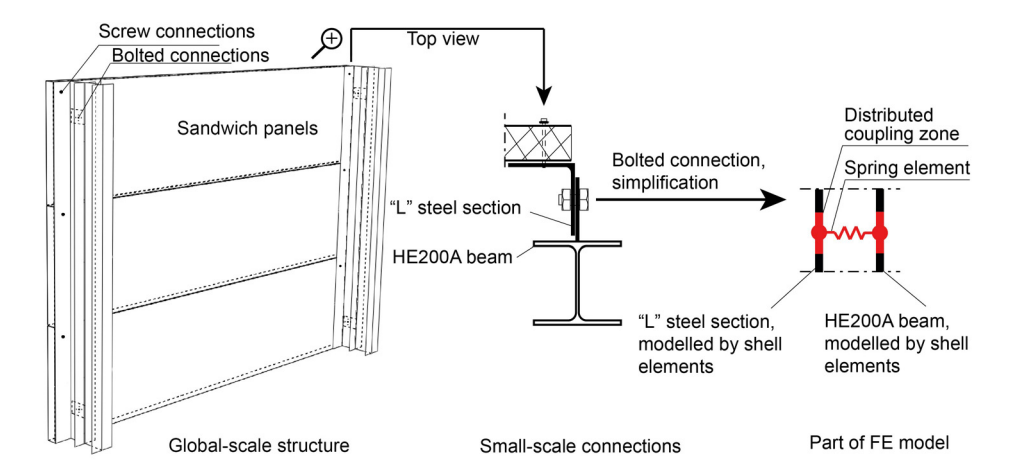


Fig. 1. Several scales of a sandwich panel system, including a detail of the common finite element modelling of a bolted connection.

have shown that the mechanical and thermal properties of components should be understood thoroughly to predict the structure's load-bearing capacity and safety level [13].

As an alternative to full-scale experiments, finite element method (FEM) simulations can be very helpful in predicting the structure's performance, however, (a) interaction between the structure and the fire; (b) interaction between structural elements at several scales; and (c) the role of critical parts (e.g. connections) should then be incorporated, as e.g. shown by [14,15]. For example, Fig. 1 on the left shows a sandwich panel system with small-scale connections (bolts and screws). Clearly, a related FEM model needs to simultaneously take into account the behavior of different components at different scales, i.e. sandwich panels on the global scale and connections on the small scale. However, the model would be computationally expensive if all components were to be modelled in full detail, e.g. by volume elements. Therefore, simplifications are normally used: The 'L' steel section and HE200A beam in Fig. 1 are modelled by shell elements, and a bolt is made by a spring element. Such an approach was successfully used by e.g. De Boer et al. [10] and Xu et al. [14,15]. Concerning the FEM, also hybrid testing should be mentioned: experiments are then carried out for the most critical parts (i.e. connections) and real-time combined by simulations for the other surrounding parts [16,17]. Alternatively, the experiments can be simulated by dedicated models, leading to virtual hybrid approaches [18]. Also, material-related multi-scale approaches have been investigated [19,20].

Many researchers have used simplified models for connections in single-scale models, via the use of spring elements, beam elements, or tie-constraints [21], the particular approach based on the level of accuracy required. Most widely used is the so-called component model, which describes a connection via a set of individual basic springlike components, with translational and rotational degrees of freedom (DOFs) [22]. The spring characteristics are based on analytical or empirical models. For example, based on tests, Swanson et al. [23] proposed a component model for full-scale T-stub connections. Bayo et al. [24] combined all relevant deformation characteristics of components into a single four-node 2D finite element. Gödrich et al. [25] implemented the behavior of T-stub connectors into the FEM as components for which their behavior is described by theoretical models. Quan et al. [26] developed a component-based beam buckling element, used in structures under fire, and its influence on the adjacent bolted connections, modelled by component-based connection elements, was investigated. Kim et al. [27] presented a "spider" component model, which ties the bolt head and bolt nut together with a beam element representing the shaft. Similarly, Verwaerde et al. [28] proposed a user-defined FEM element to model the behavior of a single-bolted joint, but nevertheless, the behavior of the connected plates, as well as other connection failures could not be determined due to a lack of detail in the model. Finally, De Boer et al. [10] used CFD and FEM models to simulate fire-structure interaction in full-scale problems. However, the behavior and failure criteria of their connections, modelled by springs, were based on failure modes at ambient temperature. This is quite a simplification, as many studies show the relevance of temperature-dependent mechanical behavior of components like connections [29,30].

In general, the above-described modelling of connections by springs cannot capture the fact that each connection, at each location and moment in time, has a unique 3D state of temperatures, displacements, and strain history. For example, the bolted connection in Fig. 1 in the middle, assumingly being in the state of a constant 400 °C and under tension, with a history of plastic strain in tension, will behave differently for a new state including shear (e.g. due to thermal expansion) than a similar bolt that has less plastic strain from the past. Besides, studies provide evidence that the thermal behavior and expansion of a structural system should be taken into account, the expansion strongly loading the connections. Based on experiments, in which a two-way slab and composite beam structure were subjected to fire, expansion was shown to be a critical factor [31]. After conducting a full-scale fire test of an eight-storey composite steel frame structure, Usmani et al. [32] demonstrated that thermally induced internal forces and displacements have a larger impact on the structural response than the applied loads. As the number of variations from connection state to state is infinite, and expansion on the structural level is important, it then seems that the complete structure should be modelled, including not only temperature loads, but also mechanical loads and mechanical failure modes for all connections, with all their relevant details (e.g. threads) modelled [33]. Such a detailed model for the complete structure requires an extremely fine mesh for the connections and their surroundings, which again significantly increases computational costs and memory requirements. This is even more the case if the detailed model would be part of a two-way coupled simulation approach (not presented here), with CFD fire simulations and both FEM thermodynamical and thermomechanical simulations [10].

Specifically for bolted connections, Table 3.4 in Eurocode 3, part 1-8 [34] lists five failure modes, namely tension, shear, bearing, punching, and combined shear and tension, see Fig. 2. However, some additional failure modes exist. Firstly, tear-out, which is similar to bearing, however, due to a small end distance, the shear force will shear the material between the bolt hole and the outer edge. Secondly, a small edge distance may induce net section failure. For example, Zadanfarrokh et al. [35] studied the flexibility and strength of bolted connections in cold-formed steel sections, as a function of among others the bolt diameter and type, the sheet thickness and strength, and the end distance. Their tests showed bearing, but also net section failure. Furthermore, they mentioned the trend to define bearing and sheet tearing (defined as tear-out in Fig. 2) as a single failure mode. Rogers et al.

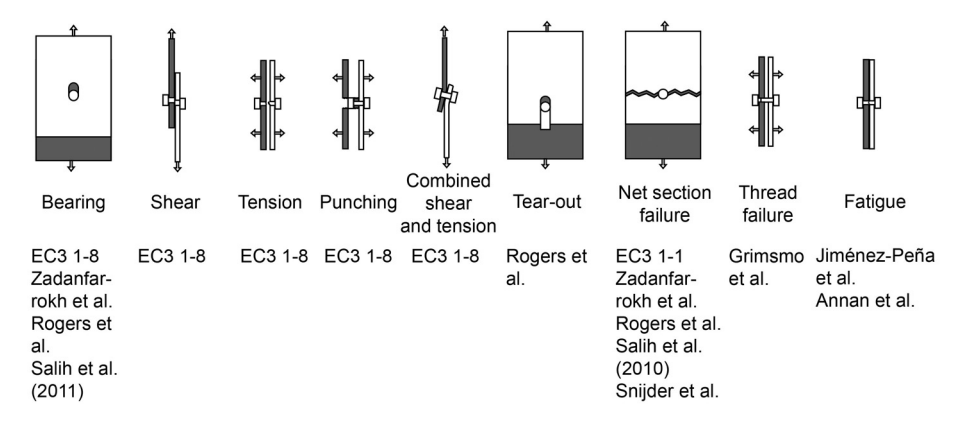


Fig. 2. Failure modes of bolted connections (references for ambient, see text for elevated temperatures).

[36] presented a study of bolted connections in shear and mentioned the failure modes end pull-out (defined as tear-out in Fig. 2), bearing, and net section failure. Salih et al. studied net section failure [37] and bearing [38]. Snijder et al. studied an extensive set of bolted connection configurations (including staggered ones) for net section failure [39]. Net section failure is handled by Eurocode 3, part 1-1 [40], however, for a single bolt, tear-out is not explicitly covered in Eurocode 3 part 1-8 [34], as end distances are controlled, however, for a row of bolts so-called block tearing is checked. Concerning thread failure, Grimsmo et al. [41] studied bolt-nut assemblies under tension. Thread failure was only observed for non-standard nut positions, whereas bolt fracture occurred in all other cases. Finally, if there is a repeated, cyclic load on a bolted connection, fatigue may occur, as researched by e.g. [42,43]. All these failure modes for ambient temperatures may also occur for elevated temperatures, e.g. under fire conditions [44]. For instance, Yan et al. [45] found a good agreement between finite element simulations and experiments of single shear bolted connections of thin sheets, with bearing and net section failure modes observed. He et al. studied thinwalled bolted plates in shear at elevated temperatures, and developed well-corresponding finite element models. Failure modes observed were net section failure, end pull-out (defined as tear-out in Fig. 2) and bearing [46]. Bull et al. studied bolt assemblies under tension in fire. They noticed that at ambient temperatures bolt fracture and thread-stripping occurred, whereas thread-stripping took place at elevated temperatures

In the third paragraph of this introductory section, three FEM requirements were mentioned. The first, (a) considering the interaction of the structure and fire, has been addressed in several publications [10,14,15,48]. This paper focuses on the latter two requirements. With respect to the second requirement, (b) taking into account interaction between structural elements at several scales, a two-scale method will be presented that can reduce computational costs and memory requirements, and provides an insightful functional separation of scales: what matters on the small scale (details) is treated separately and brought forward to the global-scale model, which captures the relevant issues on that scale, i.e. the structure. Vice versa, the behavior of the structure provides Boundary Conditions (BCs) on the small scale. For the third requirement, (c) the influence of critical parts, e.g. connections, should be incorporated, a small-scale model is introduced for which it is tried to include combinations of all essential failure modes of bolted connections, and including elevated temperatures.

In conclusion, there is a need for the correct and computationally efficient modelling of structures under fire, at different scales, including connections. The contribution of this paper is as follows. It presents a two-scale method, using a computationally as simple as possible small-scale model for a bolted connection, which still describes all essential failure modes, their combinations, including elevated temperatures. The resulting two-scale method bridges a gap between the

existing very detailed small-scale models for bolts, and the existing global-scale structural models, which use springs for the bolts. The method provides insights, since it separates the different scales functionally, enlightening their relationships. Furthermore, it allows for efficient distributed computing, handles local non-convergence (e.g. a failing bolt) naturally, and can as such be used in e.g. two-way coupled fire-structure simulations (not presented here). A similar approach has been published for screw connections [49], but note that screws and bolts have fundamentally different connection mechanisms (thread-based vs. bolt-nut-structure contacts) and related different failure modes

In the next section, the two-scale method will be described, including an overview, small-scale model simplifications, equivalent spring properties, and an explanation of submodelling as a technique to take into account the boundary conditions. Section 3 studies the modelling of the bolt itself, in the small-scale model. The proposed material model is validated by existing experiments, smooth shank modelling is verified, and temperature-dependent behavior is validated by experiments from the literature. Section 4 discusses the type of the spring element to be used in the global-scale model. Then, having set the details of the small-scale and global-scale models, in Section 5 the two-scale method is demonstrated for tension, shear, bearing, and punching. Existing experiments are used for validation and it is explained why net section failure cannot be described, which also applies to tear-out. Multi-directional load cases are introduced too, including elevated temperatures. Finally, Section 6 presents the conclusions. Open-source scripts and code have been published online, for all simulations as presented in this paper [50]. As such, all simulations can be reproduced and used for further research.

2. Description of the two-scale method.

2.1. Overview of the two-scale model. Fig. 3 (b) shows an overview of the two-scale method. It consists of a global-scale model and as many small-scale models as the number of bolt connections. For this example, the global-scale model includes two plates, each modelled by volume elements, connected by a spring element that represents the bolt. The small-scale model describes the dotted-line-indicated part in the centre of the global-scale model, again by volume elements, and it includes a bolt, also modelled by volume elements. Note that in general, the twoscale method needs a dedicated small-scale model for each unique bolted connection in the global-scale model. For instance, the method can be used for variably curved plates on the global scale, however, a dedicated small-scale model is then needed for each bolted connection at a location having a specific curvature. Fig. 3(a) shows a detailed system model. This model is used for computationally expensive verifications only, and combines the global-scale model with a bolted connection that is modelled with the same level of detail as present in the small-scale model.

Non-linear simulations usually apply the load in increments, here defined as load steps. This also applies to simulations that involve the

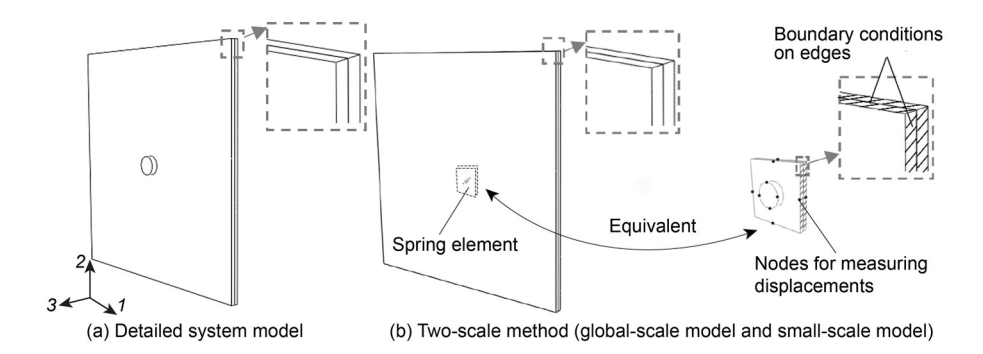


Fig. 3. Overview of the two-scale method on the right, and a detailed system model on the left, the latter for verification purposes only.

Table 1Procedures followed by the two-scale method.

Global-scale model		Small-scale model
Global-scale model load step Scripts defining global-scale model Spring stiffness initiation Output of temperature vs. time curves	$\begin{array}{c} T\\ \overrightarrow{u}\\ \overrightarrow{\phi}\\ \overrightarrow{\rightarrow} \end{array}$	Z. Transfer of BCs and temp. vs. time curves Relocation of model to location of connection in global-scale model Apply BCs and temperature vs. time curves 3. Small-scale model load step ⊤ Thermal and structural analysis of the small-scale model
5. Spring stiffness update ➤ Update stiffness of spring elements ➤ Restart analysis	<u>k</u> ←	 4. Probe step ▶ Apply pertubated boundary conditions ▶ Stiffness calculations ▶ Failure checks

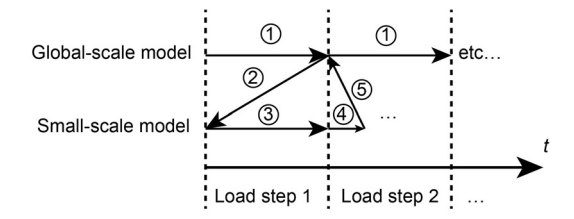


Fig. 4. Time line for two-scale method simulations.

two-scale method, where the global-scale model provides boundary conditions for the small-scale model after each load step, which in turn updates the spring properties in the global-scale model. Table 1, Figs. 3 and 4, and the description below give an overview of this coupling between the global-scale and small-scale models.

Step 1: Global-scale model load step. The global-scale and small-scale models are defined by scripts (here: Python), by which the models are also updated for all subsequent steps. First, a *linear elastic* spring element is used for the connection in the global-scale model, with its equivalent stiffness obtained in step 4 (explained later). The stiffness of the spring element is defined for three directions (i.e., three DOFs), based on a Cartesian coordinate system, and the three stiffness properties are uncoupled. Since a simulation starts with the global-scale model, the initial normal stiffness $k_{\rm bt}$ of the spring element is estimated by

$$k_{\rm bt} = \frac{E_{\rm bt} A_{\rm s}}{l_{\rm b}},\tag{1}$$

where $E_{\rm bt}$ is Young's modulus for the bolt at a specific temperature, $A_{\rm s}$ is the stress area of the threaded part and $I_{\rm b}$ is the bolt elongation length [51]. The Young's modulus has been taken as 210,000 N/mm² at room temperature and the length $I_{\rm b}$ is taken as the distance between the plate surfaces plus 1 mm at each end to account for the elastic action of the nut and head. The initial shear stiffness is assumed to be 1/3 of the tension stiffness. Note that the above stiffness values are only used for stiffness *initialisation*, and all further stiffness values follow from the

small-scale model. Detailed bolt stiffness properties as e.g. presented by [52] could be included in the initialisation stage in case a higher level of accuracy is desired. Subsequently, the global-scale model is analysed with the initial spring stiffness values. Note that if temperature loads are present, this analysis will also include the temperature vs. time data T (see also Table 1) of the nodes of the spring element.

Step 2: Transfer of BCs and temp. vs. time curves. The global and small-scale models are defined in the same global coordinate system. However, the location of the small-scale model may not automatically be such that it corresponds to the location of the connection in the global-scale model, for instance, if several connections exist at different locations. Therefore, the small-scale model may need to be translated in the coordinate system to the position of the global-scale model connection such that the correct BCs (displacements u and rotations ϕ) will be applied to the small-scale model. Additionally, the temperatures T of the nodes of the spring are projected to all nodes of the small-scale model. Accordingly, the response of the bolted connection, as presented in the next step, will include temperature-dependent effects if temperature-dependent material properties are used.

Step 3: Small-scale model load step. A structural analysis of the small-scale model, including thermomechanical aspects, is carried out in this step, to simulate the behavior of the connection and the parts of the plates modelled in the small-scale model. This step uses the same time increment as step 1, see Fig. 4.

Step 4: Probe step. Hereafter, a so-called probe step is carried out. To obtain the tangent stiffness at the end of the load step, the translational BCs are perturbed in the directions of interest, and resulting reaction force increments can be used to determine the tangent stiffness and possible failure of the connection. An additional 5% of the displacement is used here for perturbation. In the following sections, a sensitivity study on the load step size will be presented, which indirectly also verifies the sensitivity of the probe step size.

Step 5: Spring stiffness update. Now that in the small-scale model updated stiffness values have been found for the connection, the spring properties in the global-scale model can be adjusted accordingly. The global-scale model then restarts at the time where it finished before the

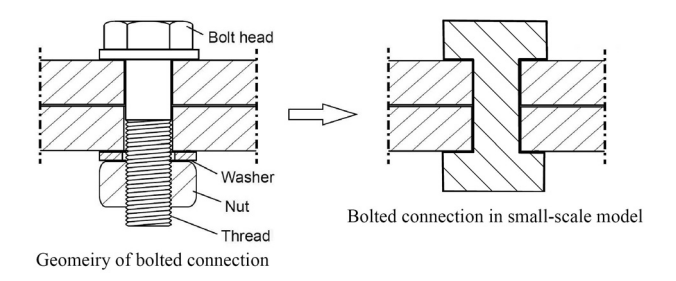


Fig. 5. Bolted connection: real, as a drawing on the left, and as finally modelled in the small-scale model on the right.

update, but using the updated (but still linear) stiffness values k for the spring. Hereafter, a new load step is carried out and the procedure starts again.

A timeline for the two-scale model is shown in Fig. 4, where the circled step numbers refer to the steps presented in this text and in Table 1.

2.2. Small-scale model simplifications. As mentioned earlier, in the two-scale method the bolt will be modelled as a spring at the global scale (like in Fig. 1), and on the small scale by using a computationally as simple as possible model, which still describes all essential failure modes, their combinations, and their temperature dependencies. Therefore, a small-scale model is suggested as shown in Fig. 5 on the right. No washers are modelled: for example Yu et al. [53] did not model the washer, but instead used the diameter of the washer for the diameter of the bolt head, and their simulations agreed well with experiments. Threads need not be modelled too, as will be shown in Section 3.2.

2.3. Equivalent spring properties. The most critical aspect of the two-scale method is the correct determination of the spring properties in the global-scale model. This section describes the derivation of the related equivalent spring properties. In general, the tangent stiffness of a spring can be approximated by Hooke's law

$$k = \frac{\Delta F}{\Delta u},\tag{2}$$

where k is the tangent spring stiffness, ΔF is a small variation of the load on the spring, and Δu is a small variation of the spring elongation or shortening. For two plates connected by a bolt, Fig. 6 shows the small-scale model on the right, and the global-scale model with a zoomed-in detail on the left. The boundary conditions for the small-scale model are the displacements (along the time of the load step) from the global-scale model at the locations coincident with the boundaries of the small-scale model. Note that snug-tight connections are considered i.e. there is no preload (tightening) of the bolt at the start of the analysis.

The variation of the load from the plates on the bolt can be measured by the variation of the contact forces in the small-scale model on the right, displayed twice: once for each type of stiffness calculation. The spring in the global-scale model has three stiffness properties: one is for the bolt axial stiffness k_3 , and two are for the representation of the shear stiffness of the bolt and the bearing stiffness of the plates, for the two independent directions k_1 and k_2 . No clearances between the bolt and the plate are modelled in the small-scale model, so the bolt head and shaft are assumed to be in full contact with the plate immediately. The contact forces are given by three force vectors for each contact pair of surfaces, i.e. $F_{1,2,3-{
m cp}1}$ for contact pair (i), modelling the contact between the bolt head and plate, and $F_{1,2,3-{
m cp}2}$ for contact pair (ii), modelling the contact between the bolt shaft and upper plate. With respect to the axial 3-direction, the deformation of the connection comes from lateral contraction of the loaded plates, or separation of the plates, and elongation of the bolt shaft. These together relate to the average of four displacements read at the red locations at the top of the bolt \overline{u}_{3a} and four displacements at the red locations at the bottom of the nut \bar{u}_{3b} as depicted in Fig. 6. The deformation of the connection then reads $\overline{u}_{\rm bolt} = \overline{u}_{\rm 3a} - \overline{u}_{\rm 3b}$. As such, using a probe step as mentioned earlier, the tangent spring stiffness k_3 can be found by:

$$k_3 = \frac{F_{3-\text{cp1(probe)}} - F_{3-\text{cp1(load)}}}{\overline{u}_{\text{bolt(probe)}} - \overline{u}_{\text{bolt(load)}}},$$
(3)

With respect to shear in the tangential 1-direction, the corresponding displacement is found via the average of the shear deformations of the two plates at the left $(u_{1a}-u_{1b})$, using the blue dot locations, and at the right $(u_{1c}-u_{1d})$, yielding $\overline{u}_{1,\text{plate}}=[(u_{1a}-u_{1b})+(u_{1c}-u_{1d})]/2$. Note that as such bearing in the plates is taken into account, also if the two plates differ in thickness or for their material properties. Again using a probe step, and noting that shear forces can be present both by radial compression in contact pair (ii) and in-plane friction in contact pair (i), the resulting stiffness k_1 is determined by:

$$k_1 = \frac{(F_{1-\mathrm{cp1(probe)}} - F_{1-\mathrm{cp1(load)}}) + (F_{1-\mathrm{cp2(probe)}} - F_{1-\mathrm{cp2(load)}})}{\overline{u}_{1,\mathrm{plate(probe)}} - \overline{u}_{1,\mathrm{plate(load)}}}. \tag{4}$$

The shear stiffness in the tangential 2-direction k_2 can be calculated in a similar fashion.

The global-scale model should predict the strains in the plates near the spring connections with reasonable accuracy, because these strains relate to the boundary conditions given to the small-scale model. Therefore, the spring is not connected to a single finite node of each plate in the global-scale model, which would cause too highly concentrated force introductions, but to a set of nodes in a so-called "distributed coupling zone" instead, shown yellow in Fig. 6 on the left. All nodes in

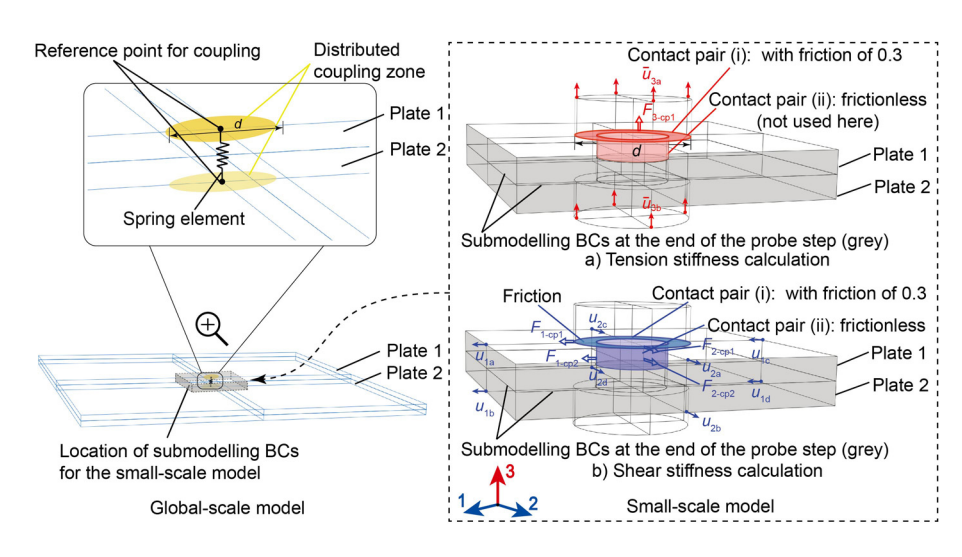


Fig. 6. Calculation of equivalent spring properties.

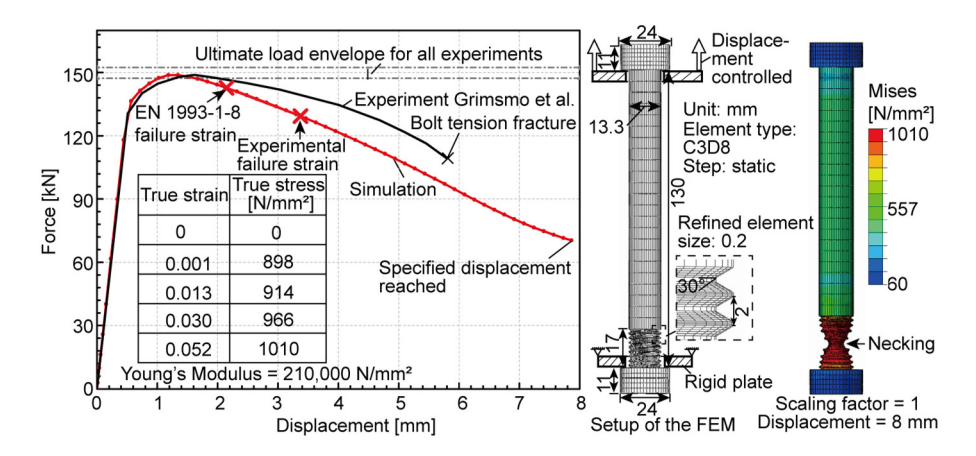


Fig. 7. M16 bolt in tension as compared with experiment.

the distributed coupling zone are rigidly connected to the node in the centre (a reference point), and subsequently the reference points of the two plates are connected by the spring element. Consequently, forces from the spring are introduced in the plates via an area whose circumference relates to the bolt shaft circumference and the bolt head and nut diameter.

2.4. Submodelling. Data transfers from the global-scale model to the small-scale model are carried out by submodeling. Originally, submodeling was conceived to provide more accurate results for a small zone within a larger model, via a finer meshed submodel [54]. Here, a submodel is used to implement the small-scale model. Submodelling is available in most finite element packages.

For submodeling, the translational and rotational DOFs from the global-scale finite element model nodes (at the imagined location of the small-scale model boundaries) need to be interpolated to the "driven" nodes (where boundary conditions are applied to) at the boundary of the small-scale model. In this research, the finite element program Abaqus [55] is used (however, other programs may allow for similar functionality, e.g. COMSOL [56] or OpenSees [57]). In Abaqus, two different methods are available for the above-mentioned interpolation: (a) solid to solid, in case volume elements are used both in the global-scale and the small-scale models; (b) shell to solid, when shell elements are used in the global-scale model while volume elements are present in the small-scale model. The accuracy of these two types of interpolation has been verified [55].

Submodelling normally functions one-directionally, from the globalscale structural model to the small-scale submodel. However, for the two-scale method, two-directional functionality is implemented, as presented in Section 2.1. This added functionality will be verified by the detailed system model.

This complete Section 2 has been dedicated to explain the setup of the two-scale method, and so the coupling between the global-scale and small-scale models. Full details can be found in the code and scripts [50], and the following two Sections 3 and 4 may additionally help to understand the backgrounds of the method: In Section 4, Fig. 15 illustrates how the spring stiffness is updated for increasing displacements.

3. Verification and validation of small-scale model. In the following, it will first be investigated whether using a material model considering plasticity but no fracture will be sufficient for bolts failing in tension. Secondly, it will be determined whether threads should be modelled or can be neglected. Note that in this section, tension cases are considered, because these are the most critical concerning the modelling of the thread. For other load cases, shear, punching, and bearing, the small-scale model is verified in Section 5, via its application in the two-scale method, using theoretical models and Eurocode predictions.

3.1. Validation of material model assumptions. Bolted connections under tension commonly fail by ductile necking and a subsequent single crack in that region. Furthermore, due to stress concentrations around the threads, local plasticity may occur before failure, and may influence the overall bolt strength and stiffness. This section studies whether it is possible to simulate the failure of a bolt in tension using a material model for plasticity, omitting the modelling of fracture. Therefore a 3D finite element simulation of an M16 bolt at room temperature under tension is presented, and results are compared with an equivalent experiment from Grimsmo et al. [41] (the experiment shown in Fig. 16(b) therein). The thread of the bolt is modelled (although not helical) to include stress concentrations. The threads between the bolt and nut are omitted by modelling the nut like a bolt head, since in practice stripping of the thread in the nut is avoided by design. The material model in the simulation uses a Von Mises yield surface with associated plastic flow and isotropic hardening. For the finite element program, the engineering stress-strain relations are converted to true stress-strain values

$$\sigma_{\text{true}} = \sigma_{\text{eng}}(1 + \varepsilon_{\text{eng}}),$$
 (5)

$$\varepsilon_{\text{true}} = \ln\left(1 + \varepsilon_{\text{eng}}\right).$$
(6)

The yield stress and hardening are defined by a multi-linear constitutive relationship, for which Fig. 7 tabulates the true strain-stress data. Note that after a true strain of 0.052, for which necking started in the material tests, the simulation keeps the true stress constant.

The curves in Fig. 7 show that the finite element model is able to predict the elastic stage, ultimate load, and plastic stage of the bolt with good accuracy. Also the necking in the experiment appears correctly in the simulation. For larger plastic deformations, however, the finite element model shows smaller displacements for the same force when compared to the experiment. This is likely due to plasticity in the threads between the bolt shank and nut. The omission of these threads in the simulation thus may underestimate the displacement at failure. Although the studied experiments failed by necking and fracture, for other (less practical) configurations in [41], threads between the bolt and nut were stripped. However, as mentioned earlier, if the bolt and nut are designed following the appropriate standards, this kind of failure should not happen.

EN 1993-1-2 [58] suggests the failure strain of steel to be 0.2, ambient, but also for elevated temperatures. This value is based on material tests in which this strain is measured over the necking region, but using a measurement length quite larger than this region itself. Consequently, actual strains in the necking region are significantly higher than measured, making the Eurocode value a quite *conservative* criterion for the actual failure strain. The value is marked in the figure, for the first occurrence in the simulation, checking all principal true tensile strains in

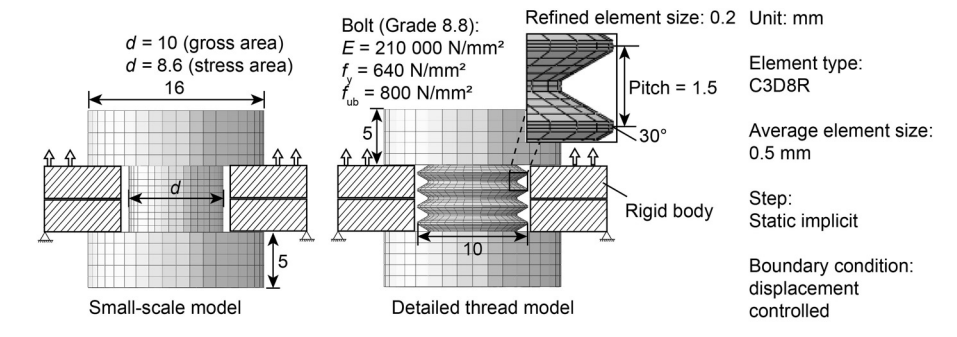


Fig. 8. Setup of the small-scale model (without threads) and the detailed thread model.

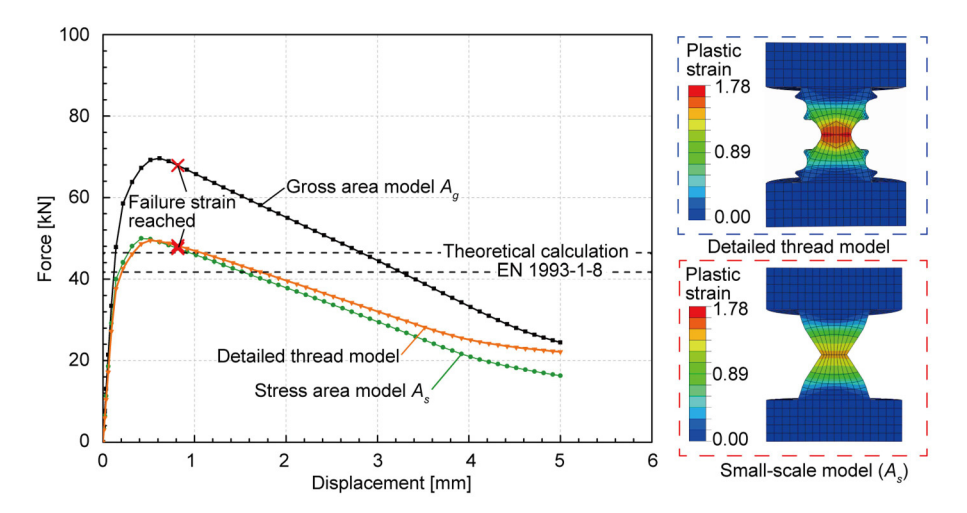


Fig. 9. Force-displacement behavior and plastic strains (deformation scale factor 1.0) for the small-scale and detailed thread models.

a contour plot based on 75% averaged nodal data. The latter means that if the difference in strain values (coming from the related elements) at a node divided by the range of strain values over the model, is smaller than 0.75, the strain values at the node are averaged into a single value. The experiment validates that failure is indeed conservatively captured with the model using this criterion. Grismo et al. carried out material tests for which speckle patterns were applied on the specimens, and images of these patterns were used to obtain the engineering strain locally, in the necking region [41]. Their value for the failure strain (0.35) is also presented, and shows a somewhat more realistic prediction of the bolt tension failure. However, it is still quite conservative, suggesting the speckle pattern measurements are able to measure strains locally but not necessarily the maximum values.

Principally, as soon as the *real* tensile failure strain is reached at any location in the finite element model, the finite element simulation should not be continued, as it does not incorporate the modelling of fracture. However, if it would be continued after the above *conservative* failure strains, it does still predict the experiment reasonably well, see the red curve after the red crosses, but further criteria are missing to predict experimental failure, as indicated by the black cross.

3.2. Verification of smooth shank modelling. The modelling of threads may be an important aspect of a bolted connection under tension, since (a) their geometry leads to stress concentrations, and (b) instead of the bolt itself, the threads in between the bolt shaft and nut may fail. This section studies whether a bolt under tension can be modelled without explicit modelling of the threads. Such a simplification is also applied in other studies [27,53,59]. If threads are omitted, the diameter of the modelled circular cross-section should be related to the real nonconstant cross-section over the bolt's length, including the effects of the related non-uniform stress distribution. The so-called stress area $A_{\rm s}$ is

used for this, which is a function of the gross area A_g and thread size and pitch, and fits simple bolt strength predictions to experimental results, e.g. [60].

In this section, the above two different cross-sectional areas for the small-scale model, Fig. 8 on the left, are compared with a detailed model that includes threads, Fig. 8 in the middle. An M10 bolt is modelled, with a pitch size according to ISO 965 [61]. Two rigid circular plates load the bolts. The lower plate is fixed, whereas the upper plate is loaded by a prescribed upward displacement equal to 5 mm. The engineering yield stress f_y adopted is $640 \,\mathrm{N/mm^2}$, and the engineering ultimate stress f_{ub} is $800 \,\mathrm{N/mm^2}$. In combination with EN 1993-1-2 [58], this leads to the ambient (20 degrees, purple) line in Fig. 11 on the left. Note that, following the previous section, true stress remains constant after the last input of the strain (i.e. 0.2 in Fig. 11).

The gross area $A_{\rm g}$ of an M10 bolt is 78.5 mm², whereas the stress area $A_{\rm s}$ equals 58 mm². As was the case in Section 3.1, also for the detailed model the bolt and nut areas are solid, as tension failure should occur in the bolt shank by design [62]. Fig. 9 presents the simulation results of the model with threads and the model without threads. It can be seen that the small-scale model using the stress area predicts similar behavior as the detailed thread model for the elastic stage, ultimate load, and post-peak behavior. To compare results with theory, the upper bound for a bolt tension failure equals the tensile strength multiplied by the stress area, which is expressed as: $F_{\rm t} = f_{\rm ub} A_{\rm s} = 46.4$ kN. This is shown in Fig. 9 with the line "Theoretical calculation". Slightly different, EN 1993-1-8 [34] predicts the ultimate load of a bolt in tension $F_{\rm t;Rd}$ by:

$$F_{t;Rd} = k_2 f_{ub} A_s = 0.9 \times 800 \times \pi \times 4.3^2 = 41.8 \text{ kN},$$
 (7)

where k_2 is a correction factor, here equal to 0.9. The ultimate loads in the simulations are slightly higher than these predicted values, probably

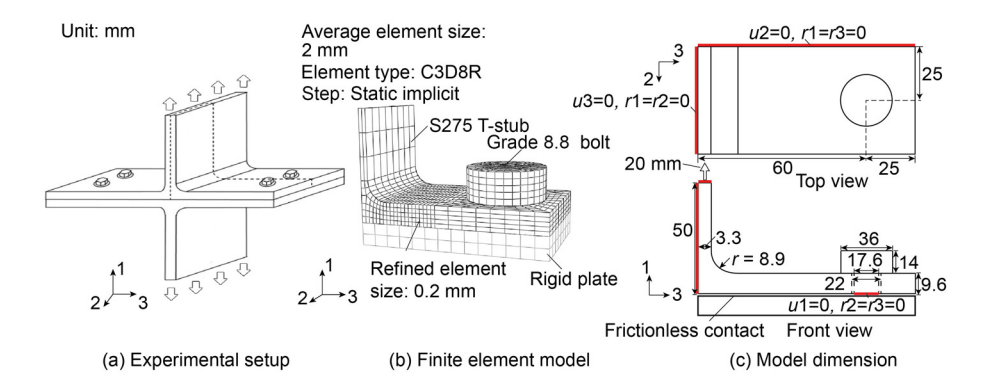


Fig. 10. Setup of Spyrou's experiments (section 4.4.1, sub-category AA in [63]) and simulations using the small-scale model.

because lateral stresses occur near the modelled bolt head and nut, due to restricted lateral contraction. As the modelled shank is quite short, these lateral stresses are also present in the failure region, and as such allow for a higher stress in load direction than the uniaxial tensile stress.

Fig. 9 on the right shows the detailed thread model and the small-scale model using the stress area, for plastic strains at the end of the simulations. Elements are distorted, and in reality, failure likely occurs before the displacements shown: In the graph on the left, the red crosses show the first occurrence of a tensile strain larger than 0.2 (as suggested by EN 1993-1-2 [58]), checking all principal true strains in a contour plot based on 75% averaged nodal data. As was shown in the previous Section 3.1, this is a conservative criterion for the actual failure strain. The small-scale model (with smooth shank) and the detailed thread model meet this criterion at the same displacement, and relatively quickly after the ultimate load, as was also seen for the experiment in the previous section.

In conclusion, the small-scale model, without threads and using the tensile stress area, behaves comparable to the detailed thread model under tension, concerning the force-displacement curve, the deformation pattern, the stress distribution, and the moment the conservative ultimate tensile strain is reached. As thread modelling is most crucial for tension, it is thus believed that in the small-scale model, the thread can be omitted for all load cases.

3.3. Validation of temperature-dependent behavior. Finally, the setup of the small-scale model is validated for temperature-dependent behavior by a comparison with experiments from the literature. Fig. 10 on the left shows specimens tested by Spyrou [63]. Two S275 T-stubs are connected by four Grade 8.8 M20 bolts and loaded under tension at different temperatures. Reportedly, failure always occurred by complete yielding of the flange followed by bolt fracture. The geometry of the finite element model is shown in Fig. 10 on the right, where the bolt consists of a solid cylinder, without threads, and a larger cylindrical part to model the bolt head, with its diameter equal to the washer under the head (36 mm). The stress area A_s for M20 bolts equals 245 mm², which results in a diameter equal to 17.6 mm. According to the symmetry of the experiment, only an eighth part is considered in the finite element model, indicated by the dotted lines in Fig. 10(a). Symmetry conditions are applied on the plates and bolt shank, shown by red lines. However, a rigid plate is modelled at the bottom of the horizontal part of the T-stub, without friction. This is because if symmetry conditions had been applied here, the T-stub would have been fixed at its bottom horizontal surface, and consequently would not have been able to open up, whereas this will occur in the experiment. Displacement control is applied on the edge of the T-stub, also indicated with a red line, with a maximal value of 20

The bolt is modelled by 8-node 3D volume elements C3D8R with a size of $3\times3\times3$ mm. The same element type is used for the T-stub, with elements $6\times6\times3$ mm. For the contact between the bolt and T-stub,

"surface to surface" contact with a so-called "finite sliding" option is used: The contact properties include the "hard contact" condition in the normal direction and a friction coefficient equal to 0.3 in the tangential directions for (a) the bolt head and the surface below, and (b) the bolt hole and the bolt shank. The material properties for the Grade 8.8 M20 bolt under ambient temperature are shown in Fig. 11 on the left. Note that similar to Section 3.1, only stress-strain data up to the necking of the coupons is used, and true stress is assumed to remain constant hereafter. Degraded properties for other temperatures are based on EN 1993-1-2 [58], as per instruction by prEN 1993-1-14 [64]. The temperature-dependent material properties of the T-stubs are taken from Fig. 16 in Yu et al. [53], and are shown in Fig. 11(b).

Fig. 12 shows that the load-deformation curves of the simulations compare well to the experiments, for different temperatures. Again, a tensile strain of 0.2 (as suggested by EN 1993-1-2) is used as a conservative prediction for failure, and the red crosses mark their first occurrence (as the maximal (so tension) principal true strain in a contour plot based on 75% averaged nodal data). Failure did not occur for 200 °C, both for the experiment and simulation. For all other temperatures, the conservative predictions seem to correlate well with the sudden load drops in the experiments. Although striking, this cannot be explained with the available information, since the experimental report does not address the load drops, and only mentions for failure the "complete yielding of the flange followed by bolt fracture". Assuming the yielding of the flange is smooth, and the bolt fracture is sudden, the latter phenomenon is the most likely suspect for the load drops. However, in the simulations, the conservative failure strain is always found in the flange, and never in the bolts, which show significantly lesser strains.

4. Verification of global-scale model (spring). The two-scale method as presented in Section 2 will be compared by a detailed system model. Using this comparison, it will be determined which type of spring is needed in the global-scale model.

4.1. Finite element models. Fig. 13 shows a finite element application of the two-scale method, with the global-scale model on the left and the for clarity enlarged small-scale model on the right. For the global-scale model, two thin plates $200 \times 200 \times 3$ mm are modelled by volume elements C3D8R, and connected by a spring element in the center. Note that the thin plates could also have been modelled with shell elements, if desired amended by a zone of solid elements around the region of interest. However, to avoid the complexities of different element types during verification by the detailed system model, which has volume elements everywhere, volume elements have also been selected here. The spring is modelled by a so-called connector element CONN3D2, which is a two-dimensional, 2-node spring element with three (translational) DOFs. Practically, this allows for modelling a stiffness for each connection in the axial and two tangential directions, which relate to one tension stiffness and two shear stiffness values, their derivation presented in Section 2.3.

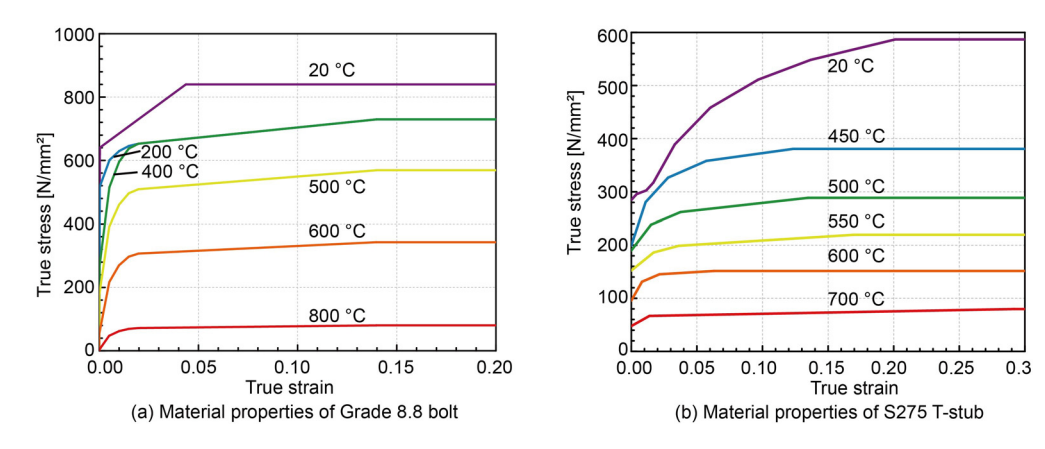


Fig. 11. Temperature dependent true stress-strain curves for the (a) Grade 8.8 M20 bolts as suggested by EN 1993-1-2 [58] and (b) T-stub S275 as used in [53].

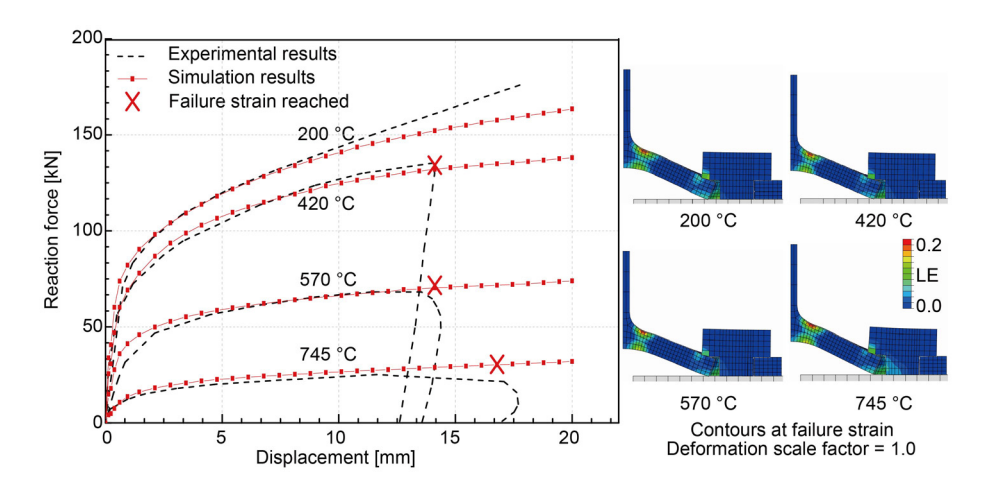


Fig. 12. Simulations of Spyrou's experiments (Fig. 4.17 in [63]).

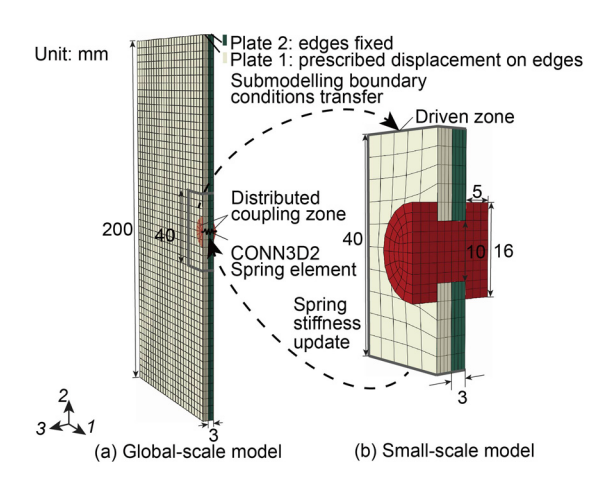


Fig. 13. Two-scale finite element model with bolted connection.

For the small-scale model, $40 \times 40 \times 3$ mm parts of the two plates are modelled by volume elements and connected by a bolt with nut, however, without modelling the threads and the washers (see Section 3). Note that for other systems the level of detail of the small-scale model can be altered. To focus on the verification of the spring, and so to avoid distraction by the expected behavior of a realistic bolt, arbitrarily bolt dimensions have been taken: the head and nut of the bolt are modelled

by two cylinders with a radius equal to 8 mm and a height of 5 mm. They are connected by a cylindrical bolt shank with a radius equal to 5 mm and a length of 6 mm.

Two types of contact are used. First, surface-to-surface contact with a friction coefficient of 0.3, applied between the plate and the bolt head (i.e. contact pair (i) in Fig. 6), and the plate and nut. Secondly, frictionless surface-to-surface contact, as applied between the two plates, and between the bolt shaft and the plates (for the plate nearest to the bolt head this resembles contact pair (ii) in Fig. 6).

All nodes on the four side surfaces (the edges) of Plate 2 (see Fig. 13) in the global-scale model are fixed for all translational DOFs. The four side surfaces of Plate 1 have a prescribed and uniform displacement, controlled via the corner points. For the upcoming simulations, an implicit static solver will be used.

4.2. Global-scale model with a linear elastic spring. The two-scale method is verified with a global-scale model with a linear elastic spring. A linearly increasing prescribed displacement is applied from 0 to 5 mm, at the four corner points of Plate 1 in the bolt's axial 3-direction, Fig. 13. As mentioned earlier, the four side surfaces (the edges) of Plate 2 are fully fixed. To provoke non-linear behavior, simultaneously a simple fire scenario is incorporated by a linearly increasing temperature starting at 20 °C and ending at 800 °C.

Linear elastic materials are used for the plates and the bolt. To study solely the bolt response, while eliminating the influence of plate action (more realistic simulations will follow), Young's modulus for the plate is a constant $2.1\times10^6~\mathrm{N/mm^2}$. For the same reason, the bolt has been given a reduced stiffness: its Young's modulus varies linearly with

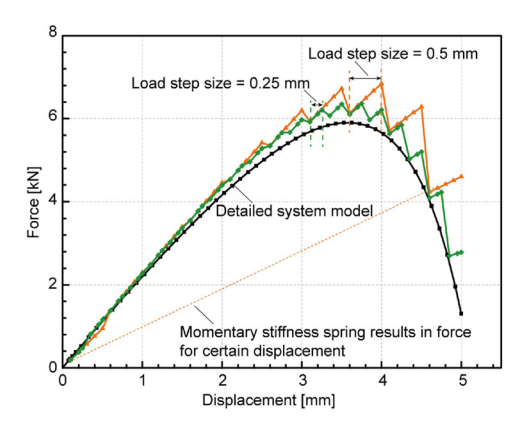


Fig. 14. Two-scale model with linear elastic spring vs. detailed system model.

the temperature, and equals $2.1\times10^3~\text{N/mm}^2$ at 20 °C and 50 N/mm² at 800 °C, whereas Poisson's ratio remains a constant 0.3 throughout the temperature range.

Thermal expansion is not included in the simulations in this paper, to obtain "pure" failure modes. However, it can easily be switched on in the models: In two-way coupled fire-structure simulations (not presented in this paper), for which the two-scale method is intended, thermal expansion has been considered in the global-scale model [10,14,15,48]. In the latter paper, the thermal expansion in the global-scale model imposes effects on the connection in the small-scale model, via mutual coupling as described in Section 2.1.

Fig. 14 shows the resulting normal force in the bolt versus the prescribed displacements of the plate corners for the two-scale method (orange and green curves) and the detailed system model (black curve).

The orange curve shows the two-scale method using load steps of 0.5 mm of prescribed displacement. For this particular simulation, each subsequent load step involves a reduction of the spring stiffness, and so the system stiffness. A sudden reduction of the force can be seen after each update of the spring stiffness. This is due to the fact that the new lower spring stiffness will result in a lower force given the prescribed displacement at that moment. To demonstrate this, an imaginary line can be drawn between the origin and a segment of choice of the orange curve, see the figure. The resulting irregular behavior can be smoothed by using smaller load steps, as is shown by the green curve, for which each load step involves 0.25 mm of prescribed displacement.

Furthermore, it can be seen that, although the *system* tangent stiffness becomes negative around 3.6 mm, as shown by the black curve of the detailed system model, the tangent stiffness of the two-scale method remains positive. As a linear spring has been used in the two-scale method, for each load step it determines the momentarily tangent stiffness, which is always positive, regardless of how small. This results in large state changes for the two-scale method at the start of each load step, even for small steps as shown by the green curve, and this may be computationally unfavourable. A more advanced spring definition can be used for improved performance, as presented in the next section.

4.3. Global-scale model with a non-linear elastic spring. This section introduces a non-linear spring for the two-scale method. Similar to the linear spring, the spring stiffness is constant within each load step, and it is updated at the start of each new load step. However, the non-linear definition allows for the inclusion of a pre-tension force f_n , also updated at the start of the load step. For the global-scale model, the force, the length change, and the stiffness of the spring in the $n^{\rm th}$ load step are given by f_n , u_n , and k_n , respectively, and the pre-tension force at the start of the $(n+1)^{\rm th}$ load step can be formulated as

$$f_{n+1} = f_n + k_n (u_{n+1} - u_n). (8)$$

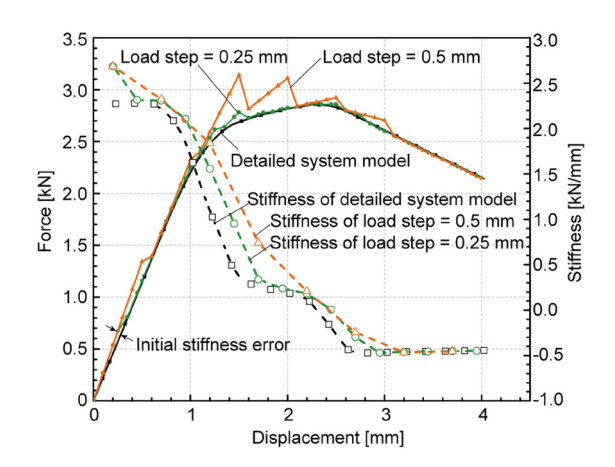


Fig. 15. Two-scale method using a non-linear spring.

At the end of each load step, the spring stiffness is determined by a probe step of the small-scale model. This spring stiffness is used for the (linear) force-displacement diagram of the non-linear spring in the global-scale model. In other words, the nonlinear spring in each load step is still using a linear stiffness, but with an offset with respect to the load.

To demonstrate this non-linear spring, the same setup is used as presented in the previous section. However, to demonstrate different types of nonlinearity, now temperatures are kept ambient, and for the bolt elastoplastic behavior will be defined: an arbitrarily selected yield stress is set to $42~\mathrm{N/mm^2}$, and the ultimate tensile strength equals $60~\mathrm{N/mm^2}$, the latter for an equivalent plastic strain equal to 0.15.

The continuous lines in Fig. 15 illustrate that the bolted connection shows first elastic and thereafter plastic behavior. The force-displacement curves of the two-scale method are reasonably close to that of the detailed system model. The spring stiffness of the initial load step is slightly different for the two-scale method and the detailed system model, due to the initial estimated stiffness values, but this difference is corrected automatically in the second load step. It can also be seen that the behavior becomes strongly non-linear as soon as the bolt starts to yield; the spring stiffness in the two-scale method is updated step by step; and the two-scale method is able to respond with a negative tangent stiffness, different from the previous section. As expected, the 0.25 mm load step size simulation (green curve) remains closer to the reference than the simulation using a 0.5 mm load step size (orange curve).

The dotted lines in Fig. 15, together with the right vertical axis, show the stiffness of the models. The two-scale method overestimates the bolt stiffness if the stifness gradient is non-zero. If wished, this can be resolved by using smaller load step sizes. Finally, note that in this Section 4, the two-scale method has been verified using a load of continuously increasing prescribed displacements or temperatures. A verification for cyclic loading-unloading schemes has been published elsewhere [14].

5. Application of the two-scale method. The two-scale method, as verified and validated in the previous sections, is applied first for single bolt connection failure modes, namely tension; shear; punching; and bearing, all at ambient temperatures. All follow the setup as presented in the above Section 4.3, including plate and bolt dimensions, and indicated if otherwise. Note that as such the diameter of the bolt, having a smooth shank, equals an arbitrary 10 mm, following Section 4.1. These applications are verified by the detailed system model and simple theoretical models, and validated by EN 1993-1-8 [34] predictions. Note that the latter two implicitly validate the small-scale models too. Then some experiments from the literature are simulated to validate the two-scale method behavior, followed by a net section failure simulation. Finally, applications that involve multi-directional loads and elevated temperatures are presented.

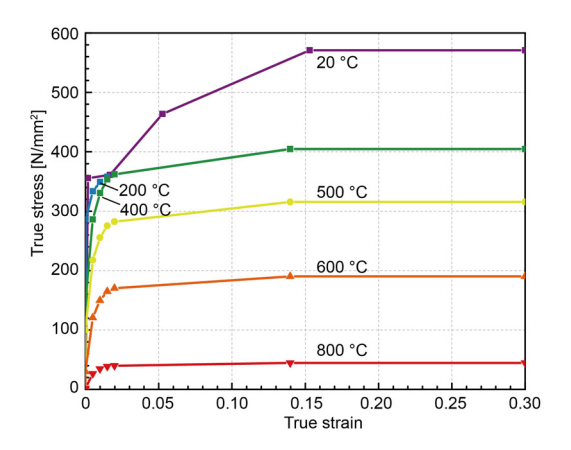


Fig. 16. Temperature-dependent true stress-strain curves of S355, following Eurocode 1993-1-2 [58].

Bolts are taken as Grade 8.8 with temperature-dependent material properties as shown in Fig. 11(a). Steel grade S355 is applied for the plates, with a yield stress of 355 N/mm² and an engineering tensile strength of 490 N/mm², both at ambient temperatures. Temperature-dependent behavior follows Eurocode 1993-1-2 [58], and resulting true stress-strain curves are shown in Fig. 16. In some simulations, linear elastic material with a Young's modulus 1000 times larger than that of steel is used for some components, e.g. the plates, to enforce ";pure" failure in other components, e.g. the bolts. As for all simulations so far, the solution is found by an implicit static method. Mentioned already in Section 3.1, the simulations are stopped as soon as a very conservative 0.2 failure strain is reached, as suggested by Eurocode 1993-1-2 [58], checking all positive principal true tensile strains in a contour plot, based on 75% averaged nodal data.

5.1. Tension. The theoretical resistance for tension is based on the equation in Section 3.2: $F_{\rm t}=f_{\rm ub}A_{\rm s}=62.8$ kN. EN 1993-1-8 [34] predicts $F_{\rm t:Rd}$ as

$$F_{\text{t:Rd}} = k_2 f_{\text{ub}} A_{\text{s}} = 0.9 \times 800 \times \pi \times 5^2 = 56.5 \text{ kN}.$$
 (9)

For pure bolt failure, the plate material is taken as linear elastic and 1000 times as stiff, in this section and the next. A prescribed displacement is applied in the bolt's axial 3-direction, on the side surfaces (the edges) of Plate 1 in the global-scale model. The load step size is 0.1 mm. Fig. 17 displays the resulting reaction force and displacement of the

Plate 1 edges, of the two-scale method and the detailed system model. It can be seen that the two-scale method and detailed system model show similar behavior for the elastic and plastic stages, and predict about the same displacement at the conservative failure strain. The differences between the two-scale method and the detailed system model for the first 0.25 mm of displacement are due to the two-scale method that needs some steps to adjust in case of large deformation rates. If wished, smaller load step sizes will resolve this issue. The simulated ultimate strength is slightly larger than the theoretical calculation due to lateral stresses related to a short bolt shank, as explained in Section 3.2.

Fig. 17 on the right shows the maximal principal logarithmic (LE) strains based on 75% averaged nodal data. These illustrate that the strain distribution of the bolt in the two-scale method is almost equal to the strain distribution in the detailed system model. The failure strain is found in the centre of the bolt. This shows that the two-scale method is not only capable of predicting the global-scale behavior, but it can also predict the strain distribution at the component level in case of tension.

5.2. Shear. An upper bound of the bolt connection's shear force can be calculated as: $F_{\rm s}=\tau_{\rm ub}A_{\rm s}$, where $\tau_{\rm ub}$ is the ultimate shear stress, which using the Von Mises criterion equals: $\tau_{\rm ub}=f_{\rm ub}/\sqrt{3}$. Using EN 1993-1-8 [34], the predicted ultimate shear resistance for a bolt can be expressed as

$$F_{v:Rd} = \alpha_v f_{ub} A_s = 0.6 \times 800 \times \pi \times 5^2 = 37.7 \text{ kN},$$
 (10)

where $\alpha_{\rm v}$ approximates $1/\sqrt{3}$, and other variables have already been defined before.

A prescribed displacement in the 1-direction, equal to 0.05 mm for each load step, is applied to the edges of Plate 1, as shown in Fig. 13. The results of the two-scale method and the detailed system model are shown in Fig. 18, which presents the resulting reaction force versus the applied displacement on the Plate 1 edges. As for tension, the two simulations yield almost identical behavior. Load step sizes could be taken smaller to improve the agreement near large changes of the spring stiffness. The model predictions are close to the theory for the ultimate force. Some elements in the bolt reach the conservative failure strain, see its definition in previous sections. Different from tension failure, these failure strains were observed along the outside of the shaft, as shown in Fig. 18.

5.3. Punching. A prescribed displacement of 2 mm per load step is applied, in the bolt's axial 3-direction, at the edges of Plate 1 (see Fig. 13) to simulate punching. The bolt material is taken as linear elastic (and 1000 times as stiff) in this section and the next, again to ensure "pure" plate failure modes. A simple theoretical model involves the perimeter

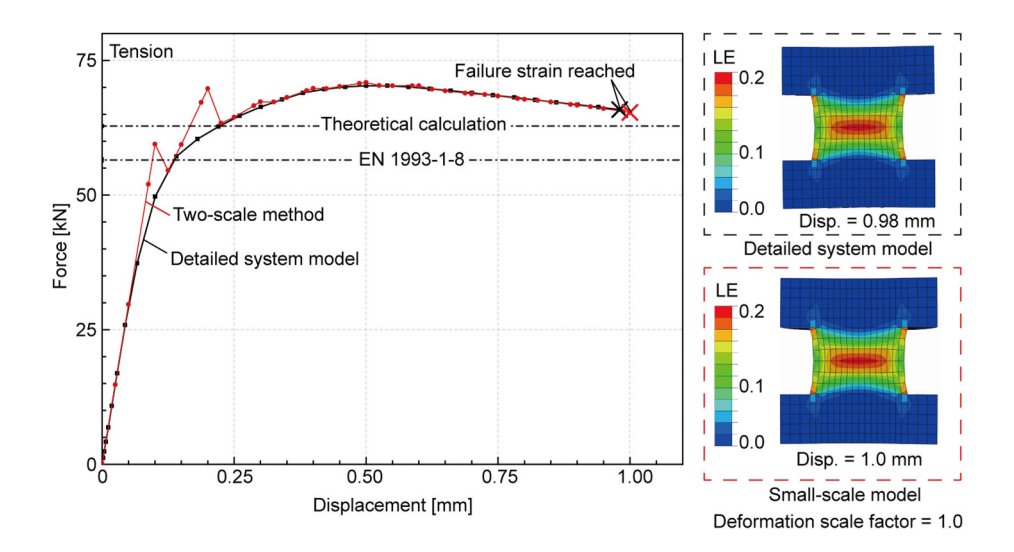


Fig. 17. Bolt tension, two-scale method vs. detailed system model.

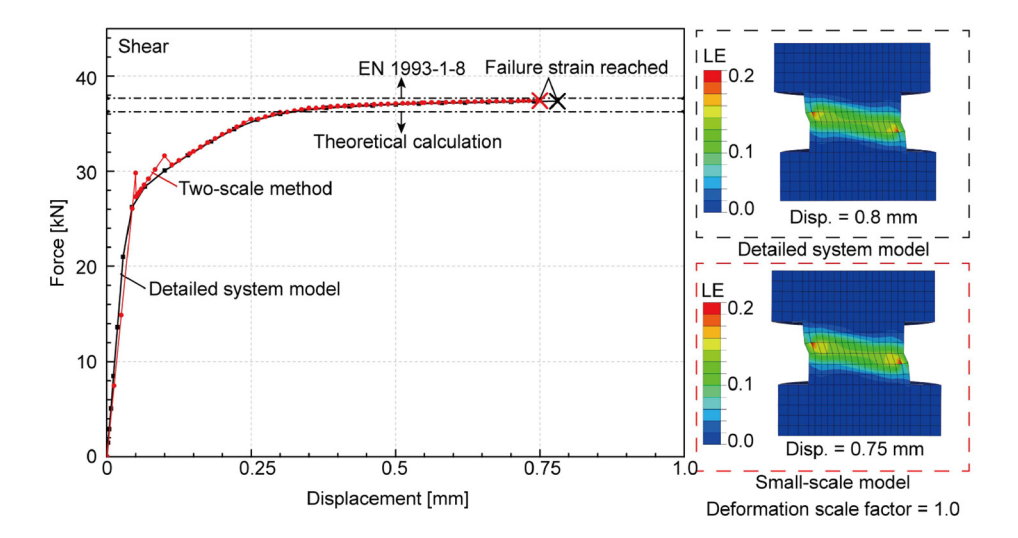


Fig. 18. Bolt shear failure, two-scale method vs. detailed system model.

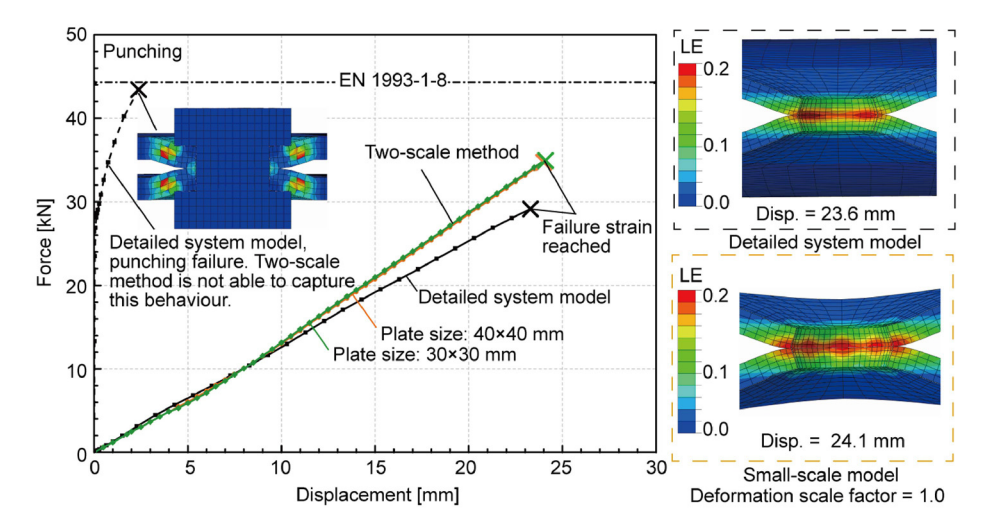


Fig. 19. Plate punching, two-scale method vs. detailed system model.

of the washer (or bolt head or nut) multiplied by the plate thickness, and this area multiplied by the shear strength, i.e.

$$F_{\rm p;Rd} = 2r\pi t_{\rm p} \Big(1/\sqrt{3}\Big) f_{\rm u} = 2\times 8\times \pi \times 3 \times \Big(1/\sqrt{3}\Big) \times 490 = 42.7~{\rm kN},~~(11)$$

where r is the radius of the washer (or bolt head or nut), $t_{\rm p}$ the plate thickness, and $f_{\rm u}$ is the engineering tensile strength of the plate. EN 1993-1-8 [34] provides a very similar equation for punching as follows:

$$F_{p;Rd} = 0.6\pi d_{\rm m} t_{\rm p} f_{\rm u} = 0.6 \times \pi \times 16 \times 3 \times 490 = 44.3 \text{ kN},$$
 (12)

where $d_{\rm m}$ is the diameter of the bolt head or nut.

Fig. 19 shows the simulation results. The two-scale method agrees well with the detailed system model at the onset of the simulation, however, the former gradually becomes stiffer. This is probably because the load introduction of the bolt on the plate is via a rigid distributed coupling zone in the global-scale model, whereas this goes via contact elements and flexible plates in the detailed system model. The detailed system model failed by non-convergence due to unresolved contact problems between the bolt head and the plate, just a little later than the moment the conservative failure strain was reached. Differently, the two-scale method was stopped manually after the conservative failure strain was observed for the first time.

Fig. 19 on the right shows contour plots of LE strains based on 75% averaged nodal data, for the final increment of the simulations. These plots indicate that no punching occurs, but plate bending, and as positive strains are plotted, yielding can be seen in the bending-related tension zones. This occurrence of bending instead of punching may explain the significant difference between the theoretical strength and the simulation results, but also the conservative failure strain may be of influence.

To provoke punching, another detailed system model is simulated, in which the plate edges are free, but a ring of nodes closely around the bolt head is fixed for the bottom plate, and a similar ring at the top plate is displaced upwards. The load-displacement curve for this simulation is shown by the black dotted line. The accompanying contour plot shows shear in the plates, and the load related to the first occurrence of the conservative tensile strain (0.2) is close to the theoretical load. This shows that the type of modelling as used in the small-scale model can handle punching. However, for the structure here, the two-scale method cannot be used. This is because the loads to be applied to the globalscale model, are within the boundaries of the small-scale model. Even if boundary conditions applied at the boundaries of the small-scale model would reflect some actions of the applied load, these boundary conditions can never apply a load within the boundaries of the small-scale model. This leads to the conclusion that the two-scale method cannot handle loads, which are always applied at the global scale, positioned within the (imaginary) boundaries of the small-scale model.

h

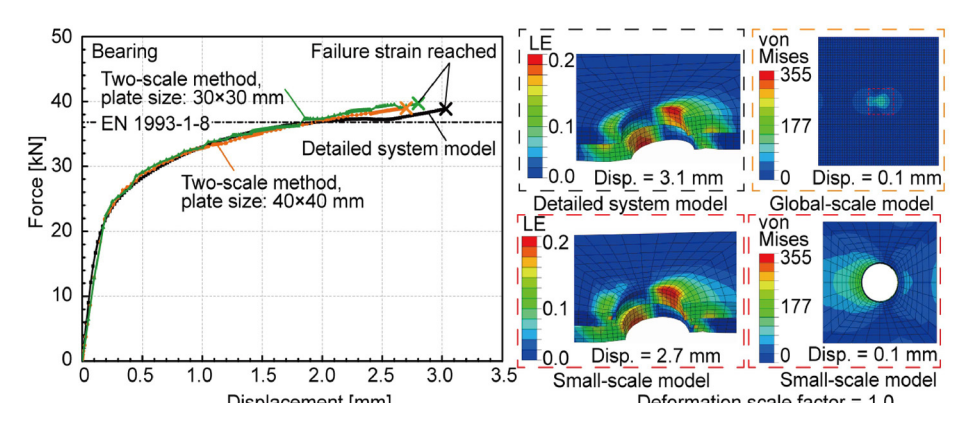


Fig. 20. Bearing, two-scale method vs. detailed system model.

These kinds of plate failure simulations need a minimum for the dimensions of the plates as modelled in the small-scale model. Therefore, without changing the dimensions of the bolt and the hole, also reduced plates 30×30 mm, three times the bolt diameter, have been tried, with the original load at the plate edges. It can be seen that in this case plates sized 30×30 mm perform similarly as the 40×40 mm plates. However, not shown here, plates 20×20 mm did not perform well, and so the standard 40×40 mm selection is considered appropriate.

5.4. Bearing. A prescribed displacement of 0.2 mm per load step is applied in the tangential 2-direction to Plate 1, see Fig. 13, to simulate bearing. Fig. 20 shows the results.

EN 1993-1-8 [34] predicts plate bearing resistance by

$$F_{b;Rd} = 2.5 f_u dt_p = 2.5 \times 490 \times 10 \times 3 = 36.8 \text{ kN},$$
 (13)

where d is the diameter of the bolt shank, $f_{\rm u}$ is the engineering tensile strength of the steel plate, and $t_{\rm p}$ is the plate thickness. It can be seen that the Eurocode prediction agrees well with the models' predicted bearing capacity. The small differences may exist because of the large number of influencing factors, such as the plate thickness, material properties, and connection method [65,66]. The two-scale method and detailed system model show comparable behavior. However, the conservative failure strain is predicted somewhat earlier in the two-scale models than in the detailed system model.

The sensitivity of the two-scale method for the size of the plates in the small-scale model is also determined for bearing. A reduction of the plates to 30×30 mm is of little influence, see Fig. 20. Not shown here, but plates with the size of 20×20 mm, two times the bolt diameter, showed significantly different behavior, namely tear-out due to the so-called edge effect [67]. Related to this, it is interesting to compare the stress fields of the global-scale and the small-scale models, Fig. 20 on the complete right. Quantitatively stresses are in the same range for both models, but, inevitably, qualitatively these are different. The small-scale model incorporates for the plate the actual hole and a real bolt to load it, whereas the global-scale model relates to a full continuous plate loaded by a spring. Most importantly, along the edges of the small-scale model, the stress field is quite similar for both models.

For an indication of computational costs, in Fig. 20 the detailed system model takes 54 minutes, whereas the two-scale model costs 78 minutes, all without multi-threading. The about 1.4 times larger costs for the two-scale method are due to the interaction between the small-scale and global-scale models, and the additional number of finite elements used. However, it should be realised that in practice multi-threading can be used, and the two-scale method has additional benefits as explained in the introduction and conclusions.

As a general conclusion for tension, shear, punching, and bearing, the two-scale method compares well to the detailed system model. Also, the two-scale method predicts plastic load-deformation curves for which their levels correspond with Eurocode predictions. The fail-

ure strain ends these plastic curves at the moment the finite element models should not be used anymore, and this is in a quite conservative fashion, as shown by the validation via various experiments in this paper.

5.5. Demonstration and experimental validation for a single load case. The previous sections demonstrated all relevant failure modes, verified by EN 1993-1-8 [34] and a detailed system model, and a validation is presented in this section. Cai et al.[68] performed a series of tests on cold-formed and stainless steel bolted lap connections, using stainless bolts, and failing by bearing. In the experiments, lips were used to prevent net section failure.

Figs. 21 and 22 on the left shows an experiment after the test: two plates with lips are connected by a M12 bolt, and the end of each plate is fixed in the test rig, so a tension force can be applied, loading the bolt in shear and tension. The overall length of each plate L_1 is 380 mm. The end distance $e_1 = 33$ mm and the edge distance $e_2 = 25$ mm. The height of the lip h equals 10 mm and its length equals $L_2 = 66$ mm. Two of these plates are connected by a bolt with a diameter d_0 of 10.3 mm. The simulation with the two-scale method is shown on the right, with material properties for the plates taken from the experiments (see Table 4 in [68]) and listed in the figure. The material properties of the bolt are taken from Fig. 11(a). Except for the experimental geometry and material properties, the two-scale method conforms to the description in Section 4.1. Results are shown in Fig. 22, which presents the two-scale method, the experiment 'L-S-1-12' [68], and additionally a detailed system model. The force-displacement diagrams of the experiment and the simulation agree well, both for the two-scale method and the detailed system model. For the simulations, using the conservative failure strain equal to 0.2, or the experimentally found 0.386 [68], both indicated by "LE" in the figure, clearly underestimates the deformation capacity, as explained earlier. If the finite element simulations are continued nevertheless, at a certain moment extreme element distortions lead to contact errors. This happens before the experiment fails, which takes place after even larger displacements.

5.6. Net section failure. Net section failure is covered by Eurocode EN 1993-1-1 [40] and the ASCE specification for the design of cold-formed stainless steel structural members [69]. Both indicate that net section failure is mainly a function of the edge distances between bolt and plate. In a study by Lu et al. [67], net section failure occurred for edge distances smaller than two times the bolt diameter. Salih et al. [37] conducted parametric studies with a finite element model to investigate the key variables affecting the failure of bolted connections, which included the edge distance e_2 and the diameter of the bolt hole d_0 (see for these variables e.g. Fig. 21). They found that net section failure occurred for an edge distance e_2/d_0 smaller than 1.5.

In order to investigate net section failure here, an additional simulation is carried out, similar to the simulation in Section 5.5, but now with all the lips removed and e_2 reduced to 15 mm. As such net section

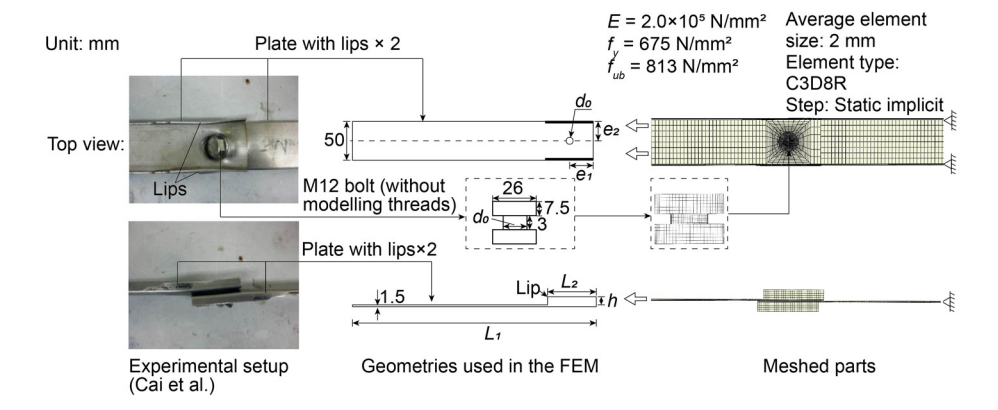


Fig. 21. Experiments Cai et al.[68] and related finite element setup.

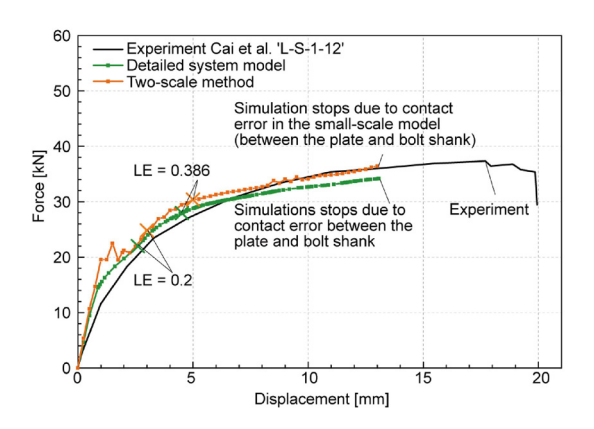


Fig. 22. Validation of two-scale model bearing failure by experiment.

failure is likely to occur. Eurocode 1993-1-1 then predicts net section failure $N_{\rm u:Rd}$ as

$$N_{\text{u:Rd}} = 0.9A_{\text{net}} f_{\text{u}} = 0.9 \times (2 \times 15 - 10.3) \times 1.5 \times 813 = 21.6 \text{ kN},$$
 (14)

ommitting the safety factor, and with $A_{\rm net}$ being the net area of the cross-section. For a theoretical prediction, the factor 0.9 in the above equation is left out, resulting in a failure load equal to 24.0 kN. Simulation results are shown in Fig. 23.

Up to 5 mm displacement (where all strains are smaller than 0.2), the small-scale method (red curve) and detailed system model (black curve) show corresponding behavior. However, for larger displacements, net section yielding, and finally failure, are predicted by the detailed system model, which models the complete structure. However, the two-scale method does not show net section failure. This should have been predicted by its global-scale model, but this model uses full cross-sections (without holes), which also include rigid distributed coupling zones (see Fig. 13). Note that it cannot be expected that the small-scale model predicts net section failure, since it does not include the edges of the plates.

From all single load cases in this Section 5, it can be concluded that the two-scale method performs well, except for net section failure, due to current limitations in the global-scale model.

5.7. Multi-directional load cases. The behavior of a bolted connection in a structure under fire relates to multi-directional loads and elevated temperatures, and an associated failure mode cannot be interpreted as one of the single failure modes presented so far. Therefore, multi-directional load cases are studied in this section.

Probing the stiffness for each direction separately, as applied in the small-scale model in previous sections, is not applicable for multidirectional load cases, as the displacements of the bolt are coupled. Therefore, a perturbation is performed in the direction of the displacement vector of the last load step, again by 5%. Subsequently, the stiffness in each direction can be determined by the procedure presented in Section 2.3. Note that if displacements in a certain direction are (almost) zero, the prediction of the stiffness is unstable due to the manipulation of very small numbers. This is not problematic though, since as soon as practically relevant displacements occur, also correct stiffnesses will be predicted, and what follows is a set of similar updates as discussed for Fig. 15.

For a demonstration of a multi-directional loading case, the two-scale method is loaded by prescribed displacement steps of 0.1 mm in the tangential 1-direction, 0.02 mm in the tangential 2-direction, and 0.6 mm in the bolt axial 3-direction, all applied to the side surfaces (the edges) of Plate 1 as explained for the single load cases. Temperature-dependent material properties for the bolt (Grade 8.8) are assigned following Fig. 11(a), but in this section the 20 °C curve is used. The two plates are using steel S355 as defined in Fig. 16 at 20 °C. As for previous sections, the simulations were stopped if at any location the conservative failure strain was recorded.

Fig. 24 shows the three independent reaction forces and their resultant vs. time (instead of displacements since the latter are different for each direction). Results are similar for the detailed system model and the two-scale method, which indicates the two-scale method performs well.

The onset of failure occurred by two-directional bearing in the plates, as was seen in the simulations, and also suggested by the curves representing the tangential directions. During this bearing, the bolt was still able to resist an about linearly increasing amount of normal force, as can be seen by the curve representing the normal direction. The conservative failure strain was first seen in the plates around the bolt hole, consistent with the bearing.

5.8. Elevated temperatures. Bolted connections behave differently for elevated temperatures, and their failure modes may change accordingly [66], so possibly this also applied to the previously presented combined load cases. The two-scale method is demonstrated here for multidirectional loads and elevated temperatures. The setup for the two-scale method is identical to the method used for the multi-direction load case in Section 5.7, except for the temperature field. With the temperature-dependent material properties as shown in Fig. 11(a) and Fig. 16, the simulation from the previous section is repeated for the following constant temperatures over time: 200 °C, 400 °C, 600 °C, and 800 °C, with results shown in Fig. 25. Detailed system model simulations are added for verification purposes.

Bearing appears the decisive failure mode at temperatures of 200 $^{\circ}$ C, 400 $^{\circ}$ C, and 800 $^{\circ}$ C, whereas the bolt fails by combined shear and tension for a temperature equal to 600 $^{\circ}$ C. This is due to the differences in material degradation for the bolt and plates as suggested in EN 1993-1-2 [58].

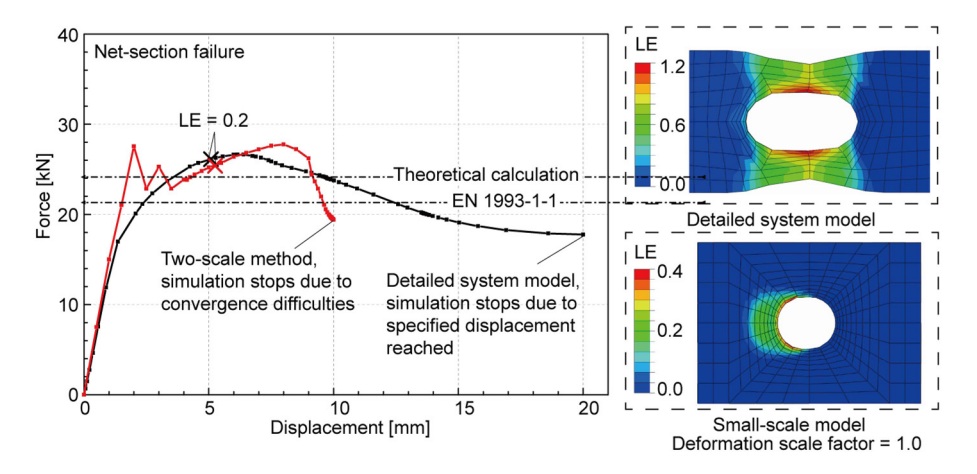


Fig. 23. Net section failure, two-scale method vs. detailed system model.

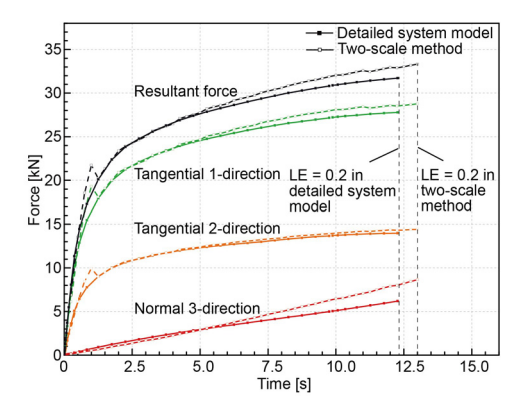


Fig. 24. Multi-directional load case, two-scale method and detailed system model.

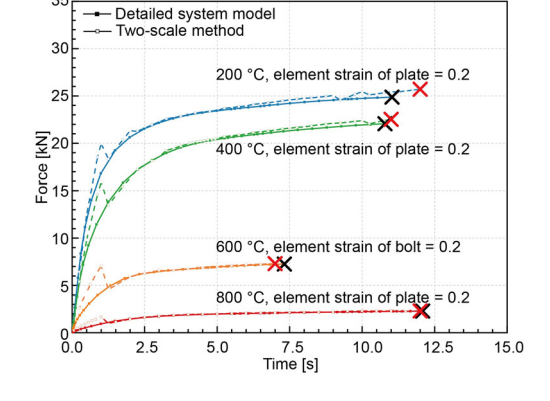


Fig. 25. Two-scale method for elevated temperatures.

6. Conclusions. There is a need for a computationally efficient bolted connection model, for the simulation of (multiple) bolted connections being part of larger structures. For this, the paper has proposed a method that is (a) two-scale, for a structured model and distributed computing, and (b) able to handle most essential bolted connection failure modes, including elevated temperatures. A possible application for the two-scale method is the use of two-way coupled fire-structure simulations.

It has been shown that the submodelling approach can be used for the two-scale method. In such a method, the small-scale model consists of a detailed model of the bolted connection with a part of its surroundings, and it uses a fine mesh to simulate the essential behavior of the connection. The connection is modelled by a spring element in the global-scale model, with the spring stiffness provided by the small-scale model.

A material model with plasticity and a smooth bolt shank (no threads) with a so-called stress area is proven effective for the small-scale model: it predicts the response of bolted connections with reasonable accuracy. The material model has been validated by existing experiments on bolt tension. However, the validation also indicated that nut thread plasticity may additionally increase connection ductility, which cannot be considered by the small-scale model. Bolts with and without modelled threads yielded similar results, which agreed reasonably well with theoretical calculations. Finally, the small-scale model is validated for its action in a structure under different temperatures by existing experiments on connected T-stubs. A material model using plasticity only cannot capture the failure deformation of a component - in this case a bolt. The state at a maximum tensile strain equal to 0.2 has been shown to give a conservative estimate of failure.

A spring in the global-scale model should be nonlinear for an optimal interaction between the small-scale and global-scale models. Practically this means that the spring uses a linear stiffness in each load step, however with an offset with respect to the load and the displacement. A real linear elastic spring (without offsets) is possible, however, will yield an irregular global force-displacement relationship, especially for a decreasing load after the ultimate load. This has been verified with a so-called detailed system model, which models the global-scale model with the level of detail found in the small-scale model, and using a parameter study on the load step size.

The two-scale method is able to describe the most essential single load case failures: tension, shear, and bearing. Also punching can be described by the small-scale model, however, for the parameter study in this paper loads had to be applied within the boundaries of the small-scale model. The aforementioned conclusions were verified by the detailed system model and comparisons with theoretical models and design standards. For plate-related failure modes (bearing and punching), a sensitivity study was carried out concerning the size of the plates in the small-scale model, and it was shown that 30×30 mm was sufficient for the considered failure modes. Existing experiments additionally validated bearing: the two-scale method fails earlier than the experiment, giving a conservative, i.e. safe prediction. The two-scale method cannot predict net section failure: the global scale model uses full cross-sections (without holes), whereas the small-scale model does not include the edges of the plates.

It has been demonstrated that the two-scale method can be used for multi-directional load cases at ambient and elevated temperatures, as

verified by a detailed system model. In the particular case demonstrated, the bolted connection fails due to bearing in two directions at ambient temperature. At elevated temperatures, plate bearing failure occurs for temperatures of 200 $^{\circ}$ C, 400 $^{\circ}$ C, and 800 $^{\circ}$ C, whereas the bolt fails in combined shear and tension for a temperature equal to 600 $^{\circ}$ C.

The research here has studied a trade-off between the computationally cheap modelling of a bolted connection (e.g. by a spring, so no failure modes and path dependency) and accuracy (e.g. by volume modelling of threads, fracture, etc.). The resulting two-scale method allows the description of basic yet essential bolted connection behavior, except nut thread and net section failure, including elevated temperatures. As such, the two-scale method may be used in e.g. computationally expensive two-way coupled fire-structure simulations, where it could be beneficial for distributed computing and densely packed bolt configurations with stiff plates, for which a single small-scale model may be representative for several connections. Related, the two-scale method has also been researched for screws [49], and as such demonstrated in two-way coupled fire-structure simulations [33] and validated by an existing experiment [14].

Declaration of competing interest

The authors declare that they have no known competing financial interests or personal relationships that could have appeared to influence the work reported in this paper.

CRediT authorship contribution statement

Qingfeng Xu: Funding acquisition, Investigation, Writing – original draft. **Hèrm Hofmeyer:** Conceptualization, Methodology, Supervision, Writing – original draft. **Johan Maljaars:** Supervision, Writing – review & editing.

Acknowledgements

This work was supported by the China Scholarship Council (Grant No. 2018-0861-0211), which is highly appreciated.

References

- G. Lou, C. Wang, J. Jiang, Y. Jiang, L. Wang, G.-Q. Li, Fire tests on full-scale steel portal frames against progressive collapse, J. Construct. Steel Res. 145 (2018) 137– 152, doi:10.1016/j.jcsr.2018.02.024.
- [2] E. Rackauskaite, P. Kotsovinos, A. Jeffers, G. Rein, Structural analysis of multi-storey steel frames exposed to travelling fires and traditional design fires, Eng. Struct. 150 (2017) 271–287, doi:10.1016/j.engstruct.2017.06.055.
- [3] A.A. Khan, S. Lin, X. Huang, A. Usmani, Facade fire hazards of bench-scale aluminum composite panel with flame-retardant core, Fire Technol. 59 (2023) 5–28, doi:10.1007/s10694-020-01089-4.
- [4] Q. Xu, H. Hofmeyer, J. Maljaars, R.A.P. van Herpen, A pyrolysis model for steel-insulation sandwich building fa/Aade systems under fire, ce/papers 6 (3-4) (2023) 2161–2166, doi:10.1002/cepa.2694.
- [5] H.H. Ghayeb, H.A. Razak, N.R. Sulong, Performance of dowel beam-to-column connections for precast concrete systems under seismic loads: a review, Construct. Build. Mater. 237 (2020) 117582, doi:10.1016/j.conbuildmat.2019.117582.
- [6] V.K.R. Kodur, M. Garlock, N. Iwankiw, Structures in fire: state-of-theart, research and training needs, Fire Technol. 48 (4) (2012) 825–839, doi:10.1007/s10694-011-0247-4.
- [7] K. Cábová, M. Garifullin, A.S. Mofrad, F. Wald, K. Mela, Y. Ciupack, Shear resistance of sandwich panel connection at elevated temperature, J. Struct. Fire Eng. 13 (2) (2021) 162–170. doi:10.1108/JSFE-03-2021-0013.
- [8] E.C. Fischer, R. Chicchi, L. Choe, Review of research on the fire behavior of simple shear connections, Fire Technol. 57 (4) (2021) 1519–1540.
- [9] J. Beitel, N. Iwankiw, Analysis of Needs and Existing Capabilities for Full-Scale Fire Resistance Testing, US Department of Commerce, Technology Administration, National Institute of standards and Technology, 2008.
- [10] J.G.G.M. de Boer, H. Hofmeyer, J. Maljaars, R.A.P. van Herpen, Two-way coupled CFD fire and thermomechanical FE analyses of a self-supporting sandwich panel façade system, Fire Saf. J. 105 (2019) 154–168, doi:10.1016/j.firesaf.2019.02.011.
- [11] Y. Liu, S.-S. Huang, I. Burgess, Investigation of a steel connection to accommodate ductility demand of beams in fire, J. Construct. Steel Res. 157 (2019) 182–197, doi:10.1016/j.jcsr.2019.02.029.

- [12] H. Hasni, P. Jiao, A.H. Alavi, N. Lajnef, S.F. Masri, Structural health monitoring of steel frames using a network of self-powered strain and acceleration sensors: a numerical study, Automat. Construct. 85 (2018) 344–357, doi:10.1016/j.autcon.2017.10.022.
- [13] T.T. Lie, Fire and Buildings, Architectural science series, Applied Science Publishers Limited, 1972.
- [14] Q. Xu, H. Hofmeyer, J. Maljaars, R.A.P. van Herpen, Full-scale fire resistance testing and two-scale simulations of sandwich panels with connections, Fire Technol. (2023), doi:10.1007/s10694-023-01463-y.
- [15] Q. Xu, H. Hofmeyer, J. Maljaars, R.A.P. van Herpen, Thermomechanical modelling of sandwich panels with connections in fire resistance tests, in: Proceedings SiF 2022-The 12th International Conference on Structures in Fire, November 30-December 2, 2022, Hong Kong, 2022, pp. 703–714.
- [16] A. Sauca, N. Mortensen, A. Drustrup, G. Abbiati, Experimental validation of a hybrid fire testing framework based on dynamic relaxation. Fire Saf. J. 121 (2021) 103315.
- [17] A. Sauca, Hybrid Fire Testing: Past, Present and Future, Springer International Publishing, Cham, 2022, pp. 275–304.
- [18] X. Cai, L. Jiang, J. Qiu, M.A. Orabi, C. Yang, G. Lou, M. Khan, Y. Yuan, G. Li, A. Usmani, Dual-3d hybrid fire simulation for modelling steel structures in fire with column failure, J. Construct. Steel Res. 197 (2022) 107511, doi:10.1016/j.jcsr.2022.107511.
- [19] T.B.Y. Chen, Multi-Scale Fire Modelling of Combustible Building Materials, The University of New South Wales, Sydney, Australia, 2022 Ph.D. thesis.
- [20] B.A. Valiente, A Multi-Scale Approach for Predicting the Fire Response of Building Barriers, Lund University, Lund, Sweden, 2021 Ph.D. thesis.
- [21] R. Garcia, M. Ross, B. Pacini, D. Roettgen, A comparative study of joint modeling methods and analysis of fasteners, Spec. Top. Struct. Dyn. Exp. Techniq. 5 (2022) 1–13.
- [22] P. Zoetemeijer, A design method for the tension side of statically loaded, bolted beam-to-column connections, HERON, 20 (1) (1974).
- [23] J.A. Swanson, R.T. Leon, Stiffness modeling of bolted t-stub connection components, J. Struct. Eng. 127 (5) (2001) 498–505, doi:10.1061/(ASCE)0733-9445(2001)127:5(498).
- [24] E. Bayo, J.M. Cabrero, B. Gil, An effective component-based method to model semirigid connections for the global analysis of steel and composite structures, Eng. Struct. 28 (1) (2006) 97–108, doi:10.1016/j.engstruct.2005.08.001.
- [25] L. Gödrich, F. Wald, J. Kabel'ač, M. Kuriková, Design finite element model of a bolted t-stub connection component, J. Construct. Steel Res. 157 (2019) 198–206, doi:10.1016/j.jcsr.2019.02.031.
- [26] G. Quan, S.-S. Huang, I. Burgess, The behaviour and effects of beam-end buckling in fire using a component-based method, Eng. Struct. 139 (2017) 15–30, doi:10.1016/j.engstruct.2017.01.076.
- [27] J. Kim, J.-C. Yoon, B.-S. Kang, Finite element analysis and modeling of structure with bolted joints, Appl. Math. Modell. 31 (5) (2007) 895–911, doi:10.1016/j.apm.2006.03.020.
- [28] R. Verwaerde, P.A. Guidault, P.A. Boucard, A nonlinear finite element connector for the simulation of bolted assemblies, Comput. Mech. 65 (6) (2020) 1531–1548, doi:10.1007/s00466-020-01833-1.
- [29] F. Liu, H. Yang, L. Gardner, Post-fire behaviour of eccentrically loaded reinforced concrete columns confined by circular steel tubes, J. Construct. Steel Res. 122 (2016) 495–510, doi:10.1016/j.jcsr.2016.04.008.
- [30] E.C. Fischer, K.L. Selden, A.H. Varma, Experimental evaluation of the fire performance of simple connections, J. Struct. Eng. 143 (2) (2017) 04016181, doi:10.1061/(ASCE)ST.1943-541X.0001664.
- [31] A.M. Sanad, J.M. Rotter, A.S. Usmani, M.A. O'Connor, Composite beams in large buildings under fire numerical modelling and structural behaviour, Fire Saf. J. 35 (3) (2000) 165–188, doi:10.1016/S0379-7112(00)00034-5.
- [32] A.S. Usmani, J.M. Rotter, S. Lamont, A.M. Sanad, M. Gillie, Fundamental principles of structural behaviour under thermal effects, Fire Saf. J. 36 (8) (2001) 721–744, doi:10.1016/S0379-7112(01)00037-6.
- [33] Q. Xu, H. Hofmeyer, J. Maljaars, A two-scale fe model to address connections in coupled fire-structure simulations, in: Proceedings Applications of Structural Fire Engineering ASFE'21, June 10-11, Ljubljana, Slovenia, 2021, pp. 388–393
- [34] EN, 1993-1-8, Eurocode 3: design of steel structures, part 1-8: design of joints, Eur. Committee: Brussels, Belgium (2005).
- [35] F. Zadanfarrokh, E. Bryan, Testing and design of bolted connections in cold formed steel sections, in: Proceedings International Specialty Conference on Cold– Formed Steel Structures, October 20-21, St. Louis, Missouri, USA, 1992, pp. 625– 662
- [36] C.A. Rogers, G.J. Hancock, Bolted connection tests of thin G550 and G300 sheet steels, J. Struct. Eng. 124 (7) (1998) 798–808, doi:10.1061/(ASCE)0733-9445(1998)124:7(798).
- [37] E. Salih, L. Gardner, D. Nethercot, Numerical investigation of net section failure in stainless steel bolted connections, J. Construct. Steel Res. 66 (12) (2010) 1455–1466, doi:10.1016/j.jcsr.2010.05.012.
- [38] E. Salih, L. Gardner, D. Nethercot, Bearing failure in stainless steel bolted connections, Eng. Struct. 33 (2) (2011) 549–562, doi:10.1016/j.engstruct.2010.11.013.
- [39] H.H. Snijder, R.W.A. Dekker, P.A. Teeuwen, 13.01: net cross-section failure of steel plates at bolt holes: numerical work and statistical assessment of design rules, ce/papers 1 (2-3) (2017) 3679–3688, doi:10.1002/cepa.424.
- [40] EN, 1993-1-1, Eurocode 3: design of steel structures, part 1-1: general rules and rules for buildings, Eur. Committee: Brussels, Belgium (2005).
- [41] E. Grimsmo, A. Aalberg, M. Langseth, A. Clausen, Failure modes of bolt and nut assemblies under tensile loading, J. Construct. Steel Res. 126 (2016) 15–25, doi:10.1016/j.jcsr.2016.06.023.

- [42] C. Jiménez-Peña, R. H. Talemi, B. Rossi, D. Debruyne, Investigations on the fretting fatigue failure mechanism of bolted joints in high strength steel subjected to different levels of pre-tension, Tribol. Int. 108 (2017) 128–140, doi:10.1016/i.triboint.2016.11.014.
- [43] R. Annan, M. Bechtold, H. Friedrich, J. Maljaars, T. Misiek, M. Paschen, Revision of EN 1993-1-11-fatigue design rules for tension components, Steel Construct. 13 (1) (2020) 61–75.
- [44] Q. Zhu, Fire Behavior of Bolted Connections, Purdue University, West Lafayette, IN, USA. 2014.
- [45] S. Yan, B. Young, Bearing factors for single shear bolted connections of thin sheet steels at elevated temperatures, Thin-Walled Struct. 52 (2012) 126–142, doi:10.1016/j.tws.2011.12.008.
- [46] Y. He, Y. Wang, Load-deflection behaviour of thin-walled bolted plates in shear at elevated temperatures, Thin-Walled Struct. 98 (2016) 127–142, doi:10.1016/j.tws.2015.02.027
- [47] L. Bull, E.J. Palmiere, R.P. Thackray, I.W. Burgess, B. Davison, Tensile behaviour of galvanised grade 8.8 bolt assemblies in fire, J. Struct. Fire Eng. (2015), doi:10.1260/2040-2317.6.3.197.
- [48] J.A. Feenstra, H. Hofmeyer, R.A.P. Van Herpen, M. Mahendran, Automated two-way coupling of CFD fire simulations to thermomechanical FE analyses at the overall structural level, Fire Saf. J. 96 (2018) 165–175, doi:10.1016/j.firesaf.2017.11.007.
- [49] Q. Xu, H. Hofmeyer, J. Maljaars, A two-scale method to include essential screw connection behaviour in two-way coupled fire-structure simulations, J. Struct. Fire Eng. (2023), doi:10.1108/JSFE-01-2023-0005.
- [50] Q. Xu, TUe-excellent-buildings/journal_paper_two_scale_method_bolted_connections_ elevated_temperatures: code_and_scripts, 2024, doi:10.5281/zenodo.10610470.
- [51] L.C. Leston-Jones, The Influence of Semi-Rigid Connections on the Performance of Steel Framed Structures in Fire, University of Sheffield, 1997 Ph.D. thesis.
- [52] C. den Otter, J. Maljaars, Preload loss of stainless steel bolts in aluminium plated slip resistant connections, Thin-Walled Struct. 157 (2020) 106984, doi:10.1016/j.tws.2020.106984.
- [53] H. Yu, I.W. Burgess, J.B. Davison, R.J. Plank, Numerical simulation of bolted steel connections in fire using explicit dynamic analysis, J. Construct. Steel Res. 64 (5) (2008) 515–525, doi:10.1016/j.jcsr.2007.10.009.
- [54] R.D. Cook, D.S. Malkus, M.E. Plesha, R.J. Witt, Concepts and Applications of Finite Element Analysis, Fourth Edition, John Wiley and Sons, Inc., Hoboken, NJ, USA, 2001
- [55] Dassault Systèmes, Abaqus, 2024, https://www.3ds.com/products/simulia/abaqus.

- [56] S. Wang, P. Ding, S. Lin, X. Huang, A. Usmani, Deformation of wood slice in fire: interactions between heterogeneous chemistry and thermomechanical stress, Proc. Combust. Inst. 38 (3) (2021) 5081–5090, doi:10.1016/j.proci.2020.08.060.
- [57] L. Jiang, Y. Jiang, Z. Zhang, A. Usmani, Thermal analysis infrastructure in opensees for fire and its smart application interface towards natural fire modelling, Fire Technol. 57 (2021) 2955–2980, doi:10.1007/s10694-020-01071-0.
- [58] EN, 1993-1-2, Eurocode 3: design of steel structures, part 1-2: general rules-structural fire design, Eur. Committee: Brussels, Belgium (2005).
- [59] R. Rahnavard, R.J. Thomas, Numerical evaluation of the effects of fire on steel connections; part 1: simulation techniques, Case Stud. Therm. Eng. 12 (2018) 445–453, doi:10.1016/j.csite.2018.06.003.
- [60] Y. Song, J. Wang, B. Uy, D. Li, Experimental behaviour and fracture prediction of austenitic stainless steel bolts under combined tension and shear, J. Construct. Steel Res. 166 (2020) 105916.
- [61] ISO, 965-2, iso general purpose metric screw threads tolerances part 2: limits of sizes for general purpose external and internal screw threads - medium quality, Switzerland (1998).
- [62] B.R. Kirby, The behaviour of high-strength grade 8.8 bolts in fire, J. Construct. Steel Res. 33 (1) (1995) 3–38, doi:10.1016/0143-974X(94)00013-8.
- [63] S. Spyrou, Development of a Component Based Model of Steel Beam-to-Column Joints at Elevated Temperatures, University of Sheffield, 2002 Ph.D. thesis.
- [64] prEN 1993-1-14, Eurocode 3 Design of steel structures Part 1-14: design assisted by finite element analysis, in preparation, Eur. Committee Standardizat.: Brussels, Belgium (2024).
- [65] B. Xie, J. Hou, Z. Xu, M. Dan, Component-based model of fin plate connections exposed to fire-part i: plate in bearing component, J. Construct. Steel Res. 149 (2018) 1–13, doi:10.1016/j.jcsr.2018.07.011.
- [66] S. Yan, B. Young, Tests of single shear bolted connections of thin sheet steels at elevated temperatures-part I: steady state tests, Thin-Walled Struct. 49 (10) (2011) 1320–1333, doi:10.1016/j.tws.2011.05.013.
- [67] W. Lu, P. Mákeläinen, J. Outinen, Z. Ma, Design of screwed steel sheeting connection at ambient and elevated temperatures, Thin-Walled Struct. 49 (12) (2011) 1526– 1533, doi:10.1016/j.tws.2011.07.014.
- [68] Y. Cai, B. Young, Structural behavior of cold-formed stainless steel bolted connections, Thin-Walled Struct. 83 (2014) 147–156, doi:10.1016/j.tws.2014.01.014.
- [69] ASCE, Specification for the Design of Cold-Formed Stainless Steel Structural Members, sei/asce 8-02, American Society of Civil Engineers, 2002, doi:10.1061/9780784405567.